

NATIONAL AERONAUTICS AND SPACE ADMINISTRATION

Technical Report No. 32-878

*Free-Flight and Free-Oscillation Techniques
for Wind-Tunnel Dynamic-Stability Testing*

Robert H. Prislin

FACILITY FORM 802

(ACCESSION NUMBER)	N66 26873	(THRU)	
(PAGES)	40	(CODE)	
(NASA CR OR TMX OR AD NUMBER)	CR-75275	(CATEGORY)	01

GPO PRICE \$ _____

CFSTI PRICE(S) \$ _____

Hard copy (HC) \$ 2.00

Microfiche (MF) .50

ff 653 July 65



JET PROPULSION LABORATORY
CALIFORNIA INSTITUTE OF TECHNOLOGY
PASADENA, CALIFORNIA

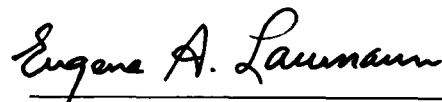
March 1, 1966

NATIONAL AERONAUTICS AND SPACE ADMINISTRATION

Technical Report No. 32-878

***Free-Flight and Free-Oscillation Techniques
for Wind-Tunnel Dynamic-Stability Testing***

Robert H. Prislin

A handwritten signature in cursive script, reading "Eugene A. Laumann". The signature is written in dark ink and is positioned above a horizontal line.

Eugene A. Laumann, Manager
Aerodynamic Facilities Section

JET PROPULSION LABORATORY
CALIFORNIA INSTITUTE OF TECHNOLOGY
PASADENA, CALIFORNIA

March 1, 1966

Copyright © 1966
Jet Propulsion Laboratory
California Institute of Technology
Prepared Under Contract No. NAS 7-100
National Aeronautics & Space Administration

CONTENTS

I. Introduction	1
II. Free-Flight Technique	2
A. Model Design and Construction	2
B. Launch Methods	3
C. Data Acquisition	5
D. Data Reduction	7
E. Dynamic-Stability Testing Capabilities	23
III. Free-Oscillation Technique	25
A. The Gas Bearing	25
B. Data Acquisition	25
C. Data Reduction	27
D. Dynamic-Stability Testing Capabilities	29
IV. Summary	29
Appendixes	30
A. Approximate Equations of Motion	30
B. Derivation of Least-Squares Equations for Nonlinear Pitching-Moment Fit	30
Nomenclature	32
References	33

TABLE

Model test characteristics	3
---	---

FIGURES

1. Free-flight model construction	3
2. Wire-release installation	4
3. Launch-tube installation	5
4. Typical high-speed motion-picture sequence	6
5. Free-flight angle-of-attack history	7
6. Data-reduction coordinate system	7
7. Plot used for calculation of drag	8
8. Comparison of linear-solution envelope to six-degree-of-freedom envelope	12
9. Representative cubic pitching moments	13

FIGURES (Cont'd)

10. k^2 vs θ_0 for various values of parameter C_{m_α}/r_m	14
11. $C_{m_{\alpha_{eff}}}$ vs θ_0 for various values of parameter C_{m_α}/r_m	15
12. θ_l/θ_n vs θ_l for various values of parameter C_{m_α}/r_m	16
13. X_n/X_l vs θ for various values of parameter C_{m_α}/r_m	17
14. θ'_l/θ'_n vs θ for various values of parameter C_{m_α}/r_m	18
15. θ'_l/θ'_n vs k^2 as a function of θ/θ_0	19
16. $\int \theta'_l d\theta / \int \theta'_n d\theta$ vs θ_0 for various values of parameter C_{m_α}/r_m	20
17. $\int \theta'_l d\theta / \int \theta'_n d\theta$ vs k^2	21
18. Correction factor R vs θ_0 for various values of parameter C_{m_α}/r_m	22
19. Correction factor R vs k^2	23
20. Comparison of cubic-solution envelope to six-degree-of-freedom envelope	24
21. The sting-supported gas bearing	25
22. Calibration sphere installation	26
23. Cutaway schematic of optron tracker	26
24. Free-oscillation amplitude vs time	27
25. Oscillograph trace of optron and strain gage output	28

ABSTRACT

26873

This Report presents the fundamentals of two wind-tunnel dynamic-stability testing techniques employed at the Jet Propulsion Laboratory: the free-flight technique, and the sting-supported free-oscillation technique. The techniques are described with reference to testing a body of revolution exhibiting planar motion. Emphasis is put on the data-reduction problem which arises when one considers nonlinear aerodynamic coefficients at arbitrary angles of attack. An approach to a general nonlinear case is outlined, and a detailed analysis is carried out for a cubic pitching-moment curve and arbitrary lift and drag curves. In addition, the advantages and disadvantages of utilizing the alternate testing methods are discussed. Possible extensions of both techniques into additional dynamic-stability testing areas are mentioned.

I. INTRODUCTION

An atmospheric entry or re-entry vehicle is likely to be initially misaligned with respect to its trajectory and, therefore, it will oscillate in an angle of attack along its flight path. This angular motion superimposed over the mean trajectory is of concern for the following reasons: (1) it affects the loads and load distribution to which the vehicle will be subjected; (2) it determines the areas of the vehicle surface which will experience the most severe heating conditions; and (3) it can affect the ability of the vehicle to perform in-flight operations such as data transmission, pre-aimed observations, and parachute deployment. When a vehicle first enters a planetary atmosphere, it experiences a positive dynamic-pressure gradient, thereby producing a continuously increasing aerodynamic static-restoring moment and a corresponding convergence of oscillation amplitude envelope. However, after peak deceleration, the dynamic pressure begins decreasing and the static-restoring moment becomes progressively weaker. If it were the only restoring moment acting, the oscillation amplitude would have to increase in order to balance energies. It is at this time during atmospheric

entry that dynamic stability coefficients may assume an important role in the determination of a vehicle's angle-of-attack history. For this reason, the problem of obtaining wind-tunnel dynamic-stability data becomes a topic of considerable interest.

Two distinct wind-tunnel testing techniques have been developed at the Jet Propulsion Laboratory: the free-flight technique, and the sting-supported free-oscillation technique. The free-flight technique refers to actual unsupported model flights in the wind tunnel. The method incorporates most of the advantages of a ballistic range, while eliminating many of the difficulties and limitations. In the majority of the free-flight development and testing done to this date, attention has been concentrated on a planar-motion situation. Recently, work has been initiated to extend the technique to a nonplanar case; however, in this Report only planar motion will be considered. The free-oscillation technique consists of a model mounted on a bearing in the wind tunnel, free to oscillate in one plane. Thus, this is a single-degree-of-freedom simulation

of a free-flying body. Sting effects inherent in this type of testing may be assessed through complementary use of the free-flight technique.

This Report describes in some detail the mechanics of both testing techniques. In the free-flight case, topics include model design criteria, launch methods, data acquisition,

and data reduction. The free-oscillation technique is described with regard to necessary hardware, data acquisition, and data reduction. Data reduction for both testing methods includes a general solution for both a linear restoring moment, and a particular nonlinear moment as well as an approach which is applicable to a more general nonlinear situation.

II. FREE-FLIGHT TECHNIQUE

A. Model Design and Construction

Unlike a ballistic range where the loadings can be as high as one-half million g's,* accelerations encountered during free-flight runs range from 10 to 100 g's. This allows much more latitude in model design and fabrication. A particular model size, material, and construction type will be dependent upon the kind of data desired and the chosen tunnel flow conditions. For example, if drag measurements were the test objective, models would be built with accelerations low enough to be compatible with material strengths and the camera-frame rate, and yet high enough to prevent excessive dropping during the trajectory across the wind-tunnel viewing window. For model design purposes only, the expected model motion may be obtained from two approximate equations of motion. Appendix A gives these equations, assumptions employed in their solutions, and resulting relations which are very useful in model-design studies.

The dynamic stability coefficient obtained from the free-flight technique is a function of the total angular decay observed during the flight. Therefore, model construction designed to optimize free-flight motion for dynamic-stability purposes would consider the following: (1) the number of oscillation cycles viewed during the flight, (2) the amplitude decay per cycle, and (3) the ability to determine this decay. The number of cycles in a given distance is proportional to

$$\left[\left(\frac{-C_{m\alpha}}{C_D} \right) \left(\frac{md^2}{I} \right) \frac{1}{d} \right]^{1/2}$$

*All symbols are defined in the Nomenclature section of this Report.

and the decay per cycle is approximately proportional to

$$\{C_{m\dot{q}} + C_{m\ddot{\alpha}}\} \left[\left(\frac{-1}{C_{m\alpha}} \right) \left(\frac{d^3}{m} \right) \left(\frac{md^2}{I} \right) \rho \right]^{1/2}$$

If the mass distribution remains fixed such that d^3/m and md^2/I remain constant as the model diameter is varied, the number of cycles varies inversely with $d^{1/2}$, while the decay per cycle varies directly with $\rho^{1/2}$. Since this implies that a smaller geometrically-similar model will have greater amplitude decay than a larger model, the diameter should be minimized, subject to the constraints of construction capabilities, photographic resolution, and ease of launch. Once the diameter and density have been fixed, the total decay for the flight can be maximized only by maximizing the model m/I^2 . This is accomplished by constructing the models of a dense inner core and a thin outside peripheral shell. The model weight (and therefore acceleration) and center-of-gravity location may be controlled by the actual size and positioning of the core within the thin shell.

The particular models tested thus far have ranged from 0.5- to 1.5-in. D. Both magnesium shells with wall thickness as low as 0.007 in. and injection molded polystyrene models with 0.020-in. wall thickness have been used. Lead, because of its density, cost, and malleability, is well-suited for the core material. Generally, 6 to 12 cycles of motion at frequencies ranging from 60 to 120 cps result. Components for typical models are shown in Fig. 1. The Table provides representative values of model test characteristics for an 0.5-in.-D blunt 10-deg cone and a 1.0-in.-D sharp 10-deg cone.

Table. Model test characteristics

Configuration	Wall material	D, in.	c.g., % ℓ	m, slugs	I, slugs-ft ²	α/g , typical	Flight time, sec
sharp cone	plastic	1.0	54.9	0.78×10^{-3}	0.10×10^{-8}	14.0	0.18
$r_n/r_b = 0.6$	magnesium	0.5	66.0	0.20×10^{-3}	0.31×10^{-7}	37.0	0.12

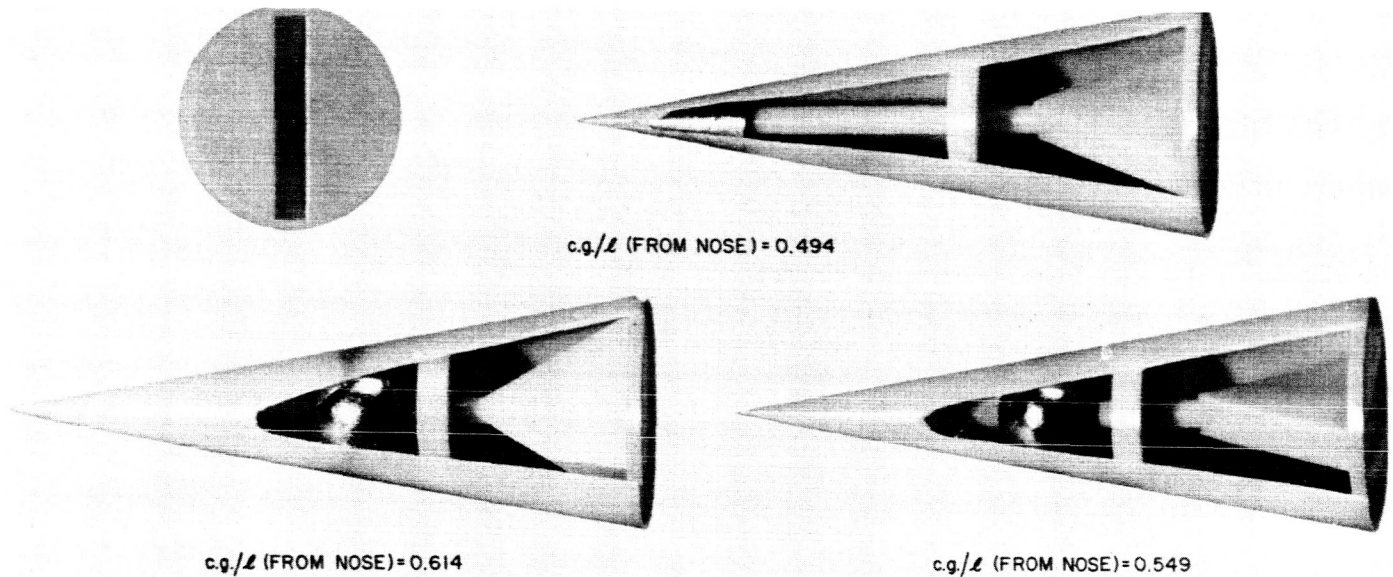


Fig. 1. Free-flight model construction

B. Launch Methods

Two actual wind-tunnel free-flight launch methods are employed. Thus far in the technique development, an attempt has been made to restrict the model to planar motion in order to greatly simplify data acquisition and reduction. In the ensuing discussions, it will generally be assumed that this restriction has been met.

In the wire-launch method the models are supported on a vertical wire at the upstream edge of the wind-tunnel viewing window. The wire itself, 0.015- to 0.030-in. D, is notched to a depth of 0.005 to 0.010 in. at a point which is subsequently located within the model. A pre-load keeps the wire in tension until it is ruptured at the notch by an impulse load, thus releasing the model into a free-flight trajectory. The wire reaction, when pulling out, seldom imparts any vertical or oscillatory motion to the model. Complete flexibility in initial angle of attack is provided by placing the wire hole through the model at the desired release angle. If the wire hole is drilled forward of the center of gravity, the model will remain stationary before rupture of the wire, and the resulting

motion will be planar. Figure 2 shows a tunnel installation of a wire-release model. The fork arrangement around the model base, as shown in this figure, provides support for the model during tunnel starting. Small clips on the wire above and below the model prevent the model from sliding on the wire prior to release.

The second method employs a pneumatic launch gun located downstream of the wind-tunnel test section. This technique allows trajectories both upstream and downstream across the viewing window, effectively doubling the test time per run. The release point is approximately 10 in. downstream of the trailing edge of the window. This insures that the model wake will be free from any influence of the projecting mechanism during the viewable trajectory. The supporting piston is extended outside the tube such that the model release occurs upstream of the tube bow shock. A set of pneumatic restraining fingers, opened just prior to model launch, provides support for the model during tunnel starting. For flat based models at angles of attack up to 30 deg, the models are mounted on a horizontal wedge fitting within the model base (Fig. 1). The wedge provides enough support during

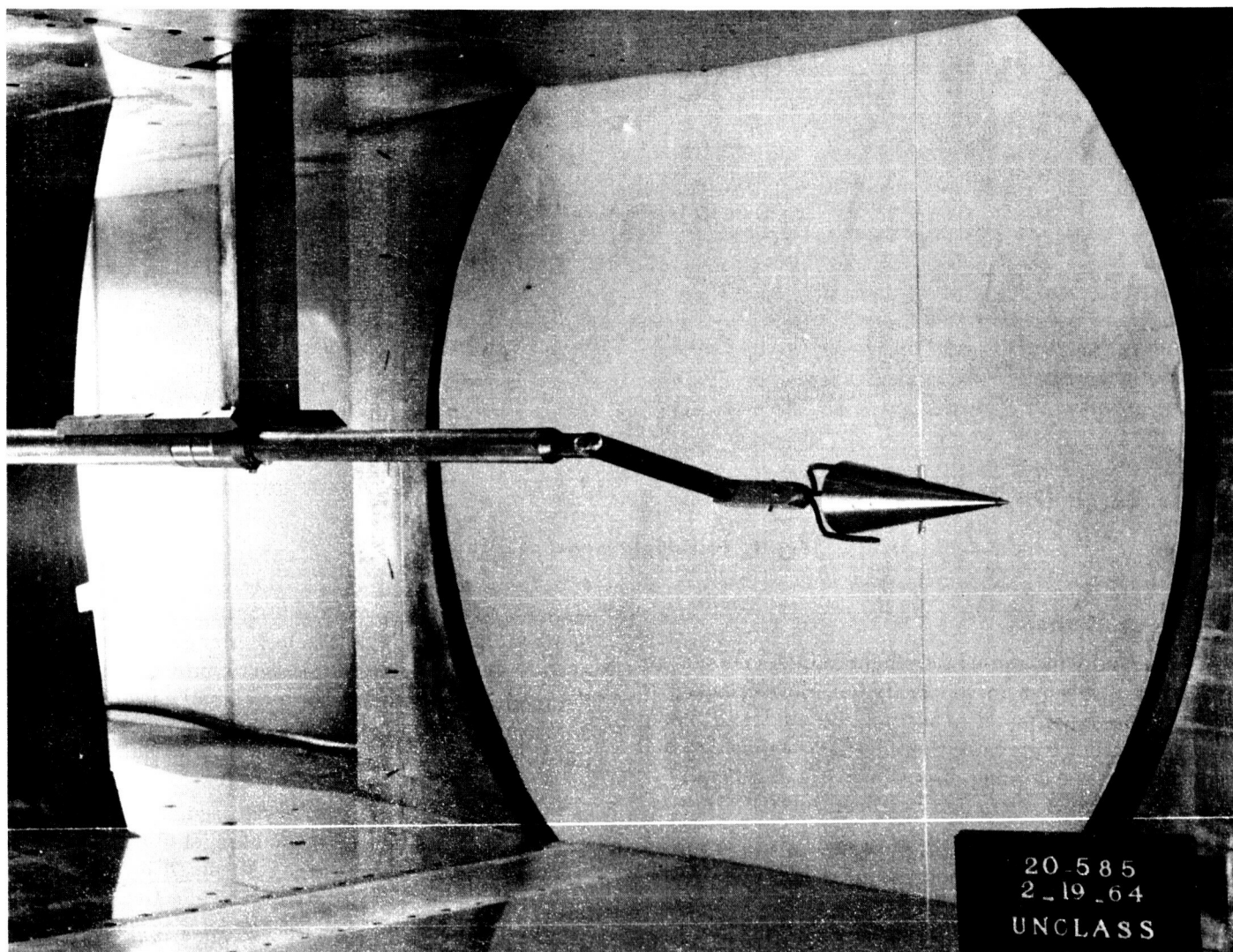


Fig. 2. Wire-release installation

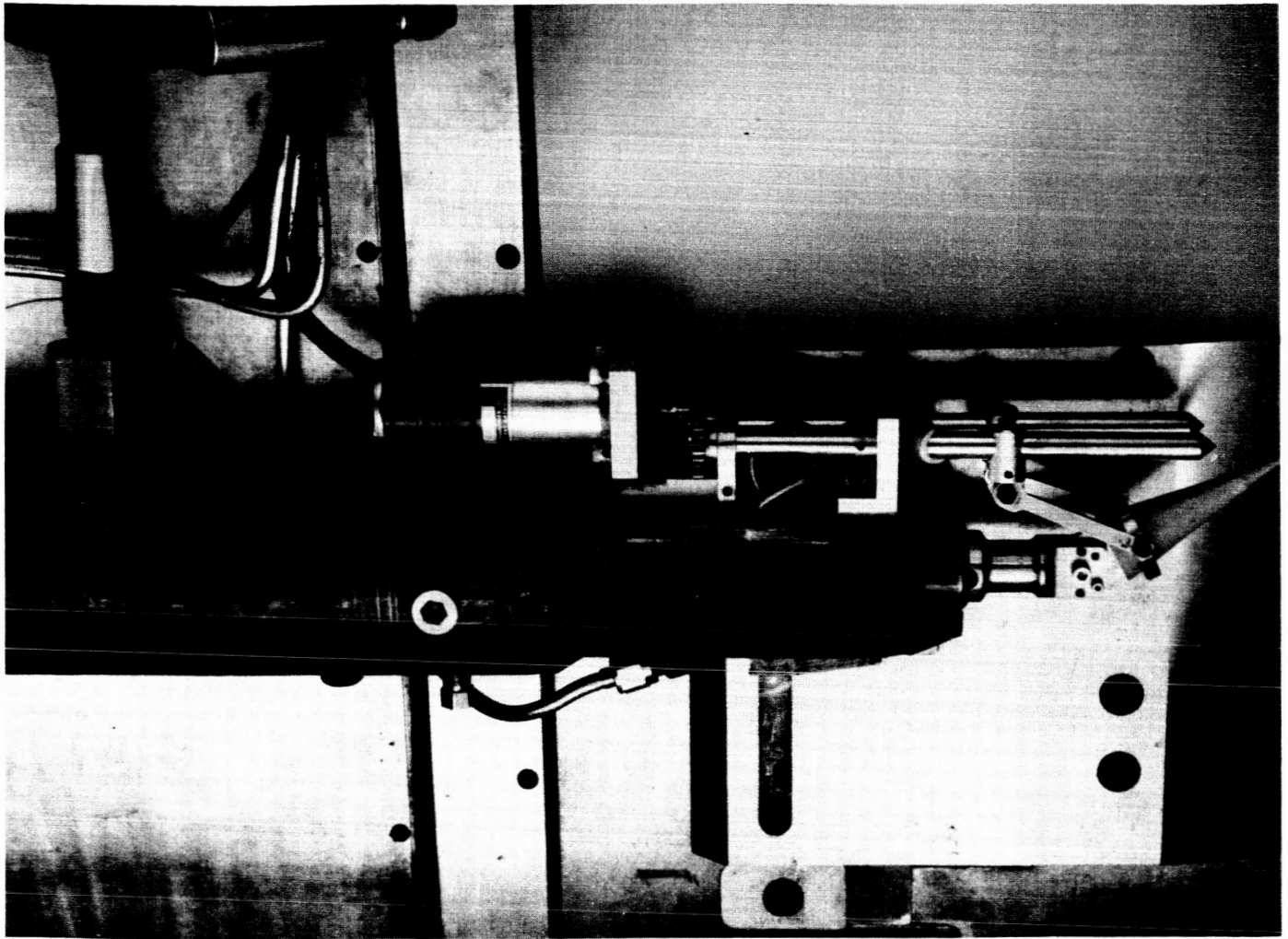


Fig. 3. Launch-tube installation

launch to insure planar motion. At larger initial angles of attack or for configurations with more complicated base geometries, a cradle support contoured to the model base and side has been used. This technique has not proved as reliable as the wedge support. Nonplanar motion has resulted about half of the time. Launch velocities vary between 20 and 100 ft/sec, depending upon the model characteristics and the tunnel flow conditions. The launch tube chamber supply pressures for required launch velocities are determined empirically. Figure 3 shows a tunnel installation of a launch-tube configuration. Further details on launching equipment for both techniques may be found in Ref. 1 and 2.

C. Data Acquisition

The model motion in the vertical plane (plane parallel with the wind-tunnel viewing window surface) is re-

corded with a high-speed (4000-5000 frames/sec) 35-mm half-frame motion-picture camera. Though the motion is normally confined to the vertical plane, a second camera is used to record the motion in the horizontal plane through a small window in the test section ceiling (JPL 20-in. supersonic wind tunnel only). At the present time, this information is used only in a qualitative sense as a verification of planar motion. In a nonplanar case, yaw angles may be measured, but because of the window size and location only about 30% of the trajectory is visible.

Generally, back lighting through the wind-tunnel schlieren system, either with or without knife edge is used. At the operating frame rates, normal exposure times would be 60 to 80 μ sec. In order to eliminate model motion during exposure, a short duration, multi-flash strobe light source is used. The flash duration can be set as low as 1.2 μ sec. A reluctance pickup on the camera sprocket

synchronizes strobe flashes with the camera shutter. By incorporating the strobe light tube into the wind-tunnel schlieren-system light house, flow-visualization pictures may be obtained and parallax distortions are eliminated.

A typical run will result in 400 to 1000 frames of data. A high-speed motion-picture sequence is shown in Fig. 4. Angular data can be determined from the film with accuracies ranging from 0.1 to 0.25 deg, depending on the

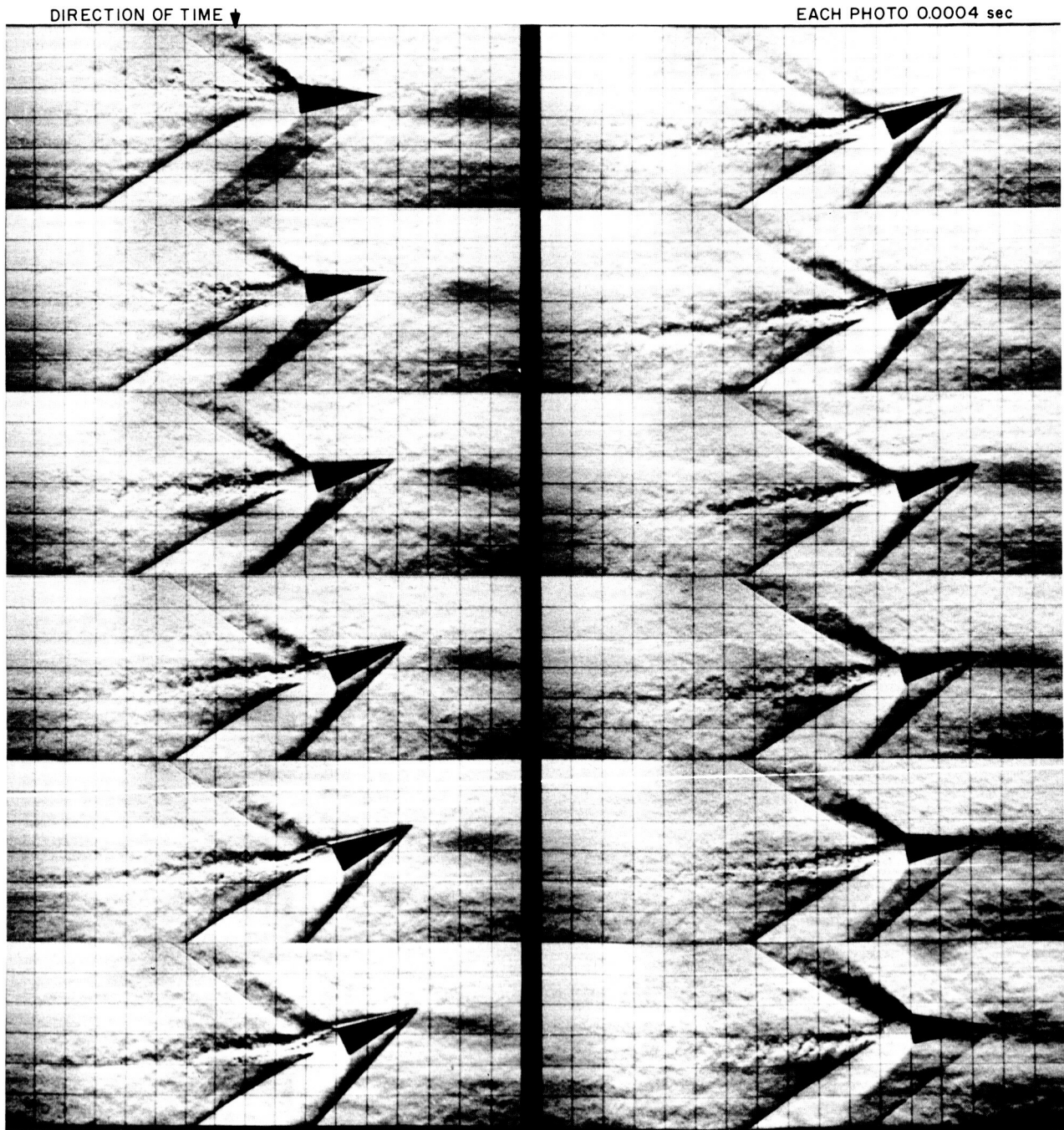


Fig. 4. Typical high-speed motion-picture sequence

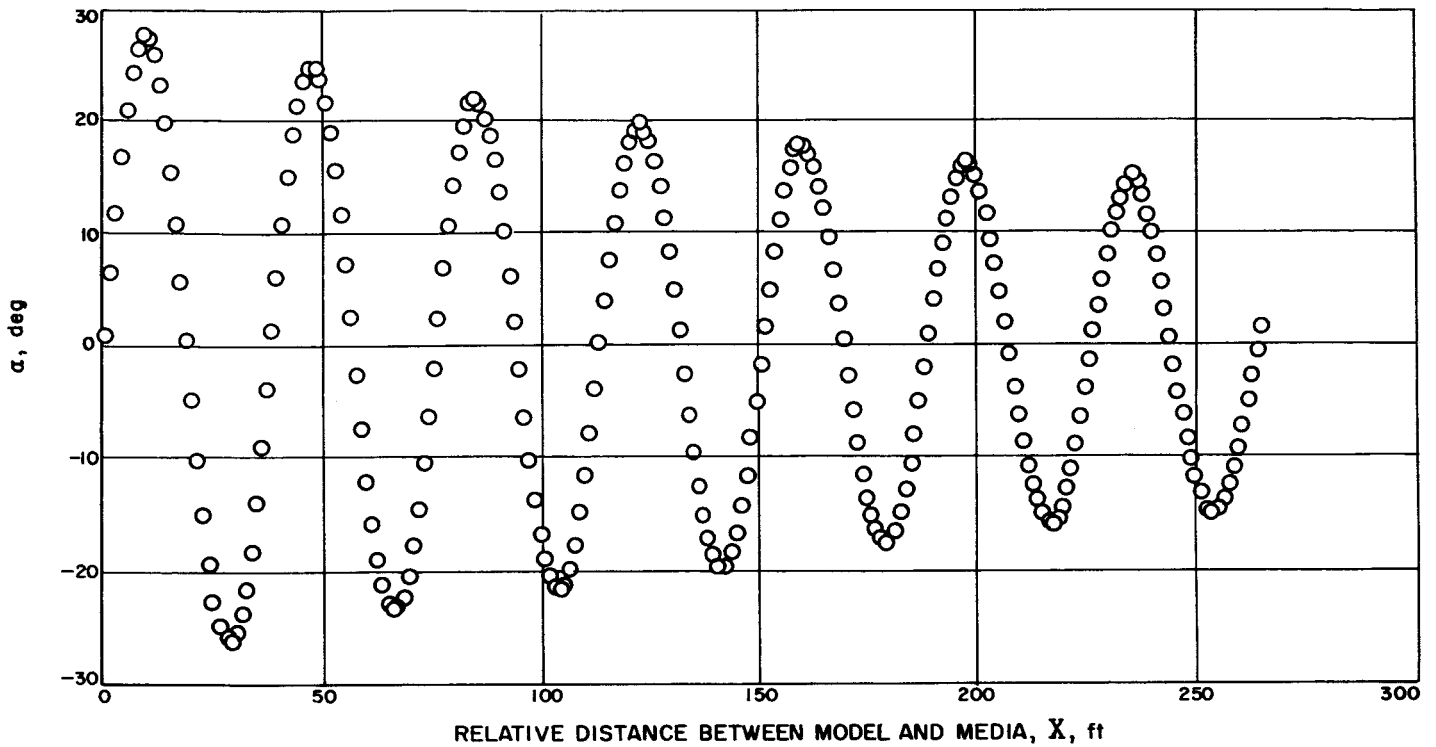


Fig. 5. Free-flight angle-of-attack history

model configuration and size. Figure 5 is a representative angle-of-attack history obtained from a test flight.

D. Data Reduction

1. Drag Data

The coordinate system used for the reduction of data (Fig. 6) is one which references the model's position to the moving gas media; X is the distance between the

model and the media and is the independent variable for the angular and translational equation of motion.

The instantaneous drag coefficient can be obtained directly from the translational equation of motion:

$$-m \frac{d^2 X}{dt^2} = \frac{1}{2} \rho V^2 A C_D$$

$$-m \frac{dV}{dt} = -m \frac{dV}{dX} \frac{dX}{dt} = -m \frac{dV}{dX} V = \frac{1}{2} \rho V^2 A C_D$$

$$C_D = \frac{-2m}{\rho A} \frac{1}{V} \frac{dV}{dX} = \frac{-2m}{\rho A} \frac{d(\ln V)}{dX}$$

This can be put into a more convenient form by noting the following:

$$\begin{aligned} \frac{d(\ln V)}{dX} &= \frac{d[\ln(V_\infty + V_m)]}{dX} = \frac{d\left[\ln\left[V_\infty\left(1 + \frac{V_m}{V_\infty}\right)\right]\right]}{dX} \\ &= \frac{d(\ln V_\infty)}{dX} + \frac{d\left[\ln\left(1 + \frac{V_m}{V_\infty}\right)\right]}{dX} \\ &= \frac{d\left[\ln\left(1 + \frac{V_m}{V_\infty}\right)\right]}{dX} \end{aligned}$$

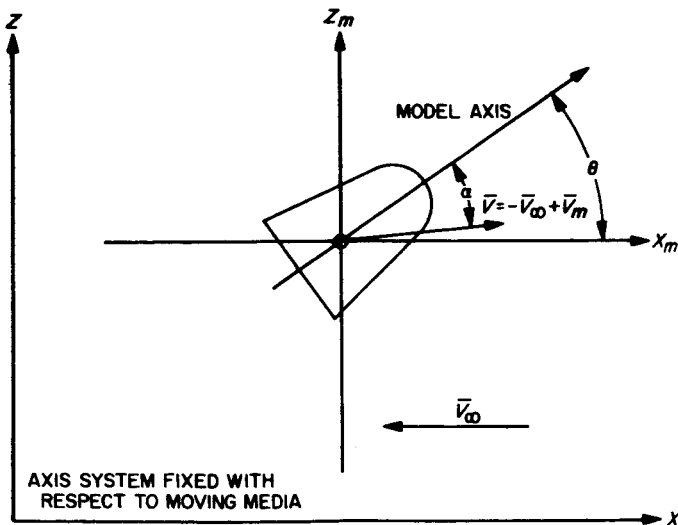


Fig. 6. Data-reduction coordinate system

Therefore,

$$C_D = \frac{-2md}{\rho A} \left[\frac{\ln \left(1 + \frac{V_m}{V_\infty} \right)}{dX} \right]$$

A linear fit through a section of the $\ln(1 + V_m/V_\infty)$ vs X data yields an effective constant drag coefficient for that section. Usually there are sufficient data at a range of amplitudes, due to the decay, to obtain several effective drag points per flight. A representative $\ln(1 + V_m/V_\infty)$ vs X plot is shown in Fig. 7.

2. Static and Dynamic Stability Data

The equation of planar angular motion is

$$I\ddot{\theta} = \frac{1}{2}\rho V^2 A d C_m + \frac{1}{2}\rho V^2 A d \{C_{m_q} + C_{m_{\dot{\alpha}}}\} \left(\frac{\dot{\theta} d}{V} \right)$$

where C_m is a function of the angle-of-attack α , and $\{C_{m_q} + C_{m_{\dot{\alpha}}}\}$ will be regarded as an effective constant coefficient over an oscillation cycle. This coefficient will vary with the oscillation amplitude. In a practical application of a solution, $\{C_{m_q} + C_{m_{\dot{\alpha}}}\}$ will be assumed constant over several cycles. Since the oscillation amplitude

will in general change in such a situation, a time-averaged amplitude will be used as a data correlation parameter. The translational equations in the X and Z directions are respectively:

$$m\ddot{X} = -\frac{1}{2}\rho V^2 A C_D \text{ and } m\ddot{Z} = \frac{1}{2}\rho V^2 A C_L mg$$

For an axisymmetric body with first-order linear aerodynamic coefficients ($C_m = C_{m_\alpha}\alpha$; $C_L = C_{L_\alpha}\alpha$; $C_D = C_{D_0}$) and small angular excursions, the equation of motion reduces to a second-order linear differential equation with constant coefficients. The solution to this equation is

$$\theta = \theta_0 e^{\lambda X} \cos \left[\left(\frac{-\rho A d}{2I} C_{m_\alpha} + \lambda^2 \right)^{1/2} X \right] \quad (1)$$

where

$$\lambda = \frac{\rho A}{4m} \left[C_{D_0} - C_{L_\alpha} + \frac{md^2}{I} \{C_{m_q} + C_{m_{\dot{\alpha}}}\} \right]$$

In general $(-\rho A d / 2I) C_{m_\alpha} > \lambda^2$ and therefore

$$C_{m_\alpha} \approx -2I / \rho A d \Omega^2$$

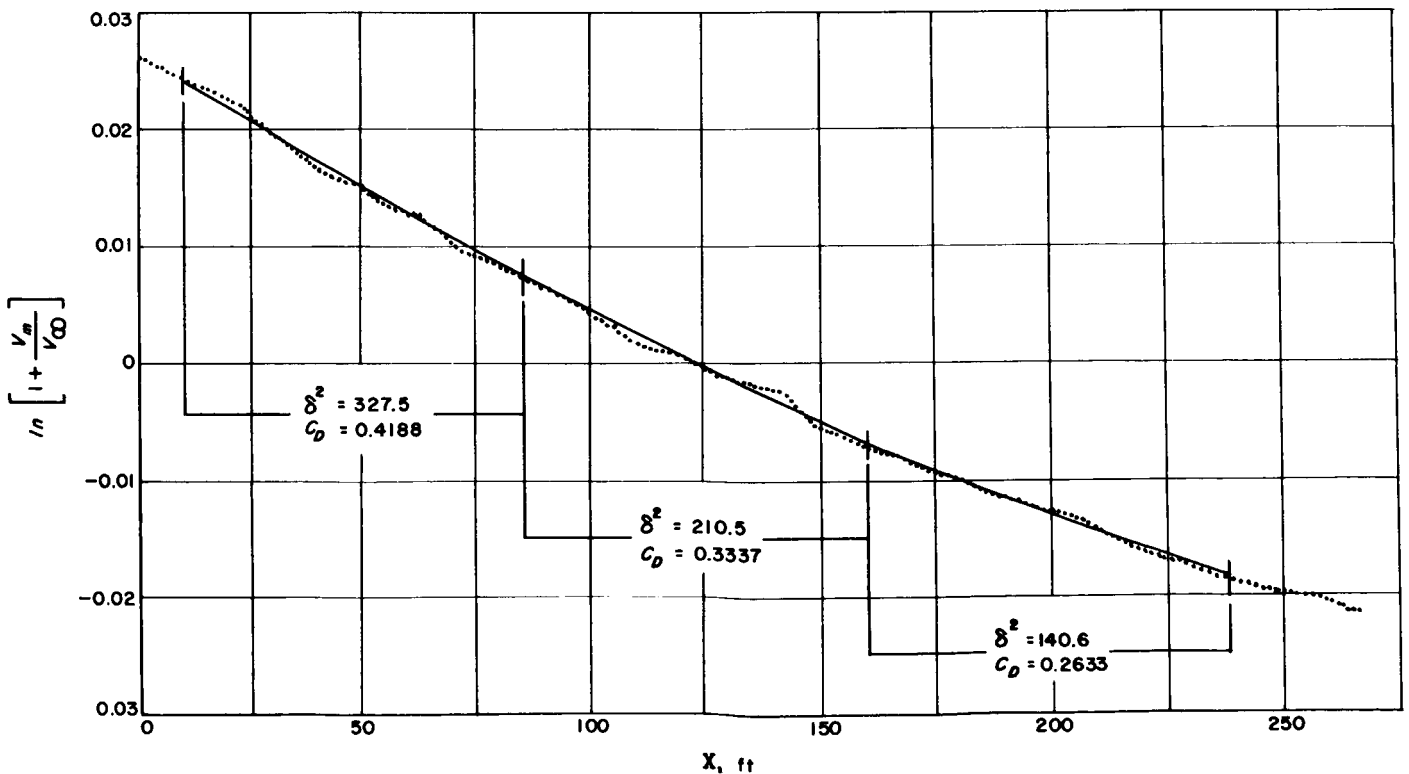


Fig. 7. Plot used for calculation of drag

where Ω is the experimental distance frequency of oscillation in rad/ft. The dynamic stability coefficient may be obtained from the amplitude envelope:

$$\{C_{m_q} + C_{m_{\dot{\alpha}}}\} \frac{md^2}{I} = \frac{4m}{\rho A} \frac{1}{(X - X_0)} \ln \left(\frac{\theta_z}{\theta_0} \right) + C_{L_\alpha} - C_{D_0}$$

where θ_z is the particular amplitude corresponding to the distance X , and θ_0 is the amplitude at $X = X_0$.

However, the conditions imposed on this solution are in general too restrictive, and more applicable solutions must be found. An unrestricted integral equation for determining the dynamic stability coefficient from energy considerations has been developed in Ref. 3:

$$\{C_{m_q} + C_{m_{\dot{\alpha}}}\} = \frac{-\frac{md}{I} \int_{-(\theta_0 - \delta\theta)}^{\theta_0} C_m(\alpha) d\theta - \int_{-(\theta_0 - \delta\theta)}^{\theta_0} C_D(\alpha) \theta' d\theta}{\frac{md^2}{I} \int_{-(\theta_0 - \delta\theta)}^{\theta_0} \theta' d\theta} \quad (2)$$

$$\{C_{m_q} + C_{m_{\dot{\alpha}}}\} \frac{md^2}{I} = \frac{-\frac{md}{I} \int_{-(\theta_0 - \delta\theta)}^{\theta_0} C_m(\theta) d\theta + \frac{\rho A d}{2I} \int_{-\theta_0}^{\theta_0} \frac{dC_m(\theta)}{d\theta} \int_{\theta_0}^{\theta} \frac{C_L(\theta)}{\theta'} d\theta d\theta - \int_{-\theta_0}^{\theta_0} C_D(\theta) \theta' d\theta}{\int_{-\theta_0}^{\theta_0} \theta' d\theta} \quad (3)$$

where θ_0 is the initial amplitude, $-(\theta_0 - \delta\theta)$ is the amplitude after one half cycle, C_m and C_D are functions of α , and $\{C_{m_q} + C_{m_{\dot{\alpha}}}\}$ is an effective constant coefficient. Using a small angle assumption and ignoring gravity

$$(\alpha - \theta) = \frac{-\dot{Z}}{V} = -\frac{dZ}{dX} \frac{dX}{dt} \frac{1}{V} = -Z'$$

From the lift equation,

$$\ddot{Z} = \frac{dZ}{dt} = \frac{d(Z'V)}{dX} V = \frac{\rho V^2 A}{2m} C_L(\alpha)$$

$$Z' = \int_{\theta_0}^{\alpha} \frac{\rho A}{2m} C_L(\alpha) dX = \frac{\rho A}{2m} \int_{\theta_0}^{\alpha} \frac{C_L(\alpha)}{\theta'} d\theta$$

Therefore,

$$\alpha = \theta + (\alpha - \theta) = \theta - \frac{\rho A}{2m} \int_{\theta_0}^{\alpha} \frac{C_L(\alpha)}{\theta'} d\theta$$

Expanding $C_m(\alpha)$ in a Taylor series about θ , and considering only the first order derivatives,

$$C_m(\alpha) = C_m(\theta) - \frac{\rho A}{2m} \frac{dC_m(\theta)}{d\theta} \int_{\theta_0}^{\alpha} \frac{C_L(\alpha)}{\theta'} d\theta$$

The lift and drag coefficients will be assumed to be functions of θ directly instead of α . This is equivalent to saying the second terms in their Taylor series expansions are quite small. Since, in general, lift and drag have second-order effects on the amplitude decay, small errors in their contributions will lead to a negligible error in the final solution for $\{C_{m_q} + C_{m_{\dot{\alpha}}}\}$. Furthermore, since the decay is very small ($\delta\theta \ll \theta_0$) in all terms except for the term containing the prime moment function $C_m(\theta)$ (that is, in all the second-order terms), the lower limit of integration $-(\theta_0 - \delta\theta)$ will be replaced by $-\theta_0$. Again, the error introduced by this approximation will be a small part of a second-order effect. Introducing these approximations into Eq. (2) results in a working form of the energy integral equation:

In solving particular problems with this energy integral equation, it will be assumed that the body's angular velocity θ' is a function primarily of the pitching moment, and that other contributors can be neglected. In the linear case, this is equivalent to the condition $\lambda^2 \ll -\rho A d / 2I \times C_{m_\alpha}$. In most physically probable situations this assumption proves excellent. In the rare case where the decay factor λ has a significant effect on the angular velocity, a simple iteration could be used to obtain θ' . In general then, an approximation for θ' may be obtained by considering the equation of motion with distance as the independent variable, ignoring all terms except the pitching moment

$$I\ddot{\theta} = \frac{1}{2}\rho V^2 A d C_m(\theta)$$

$$V^2 \theta'' + \theta' \ddot{X} = \frac{\rho A d}{2I} V^2 C_m(\theta)$$

$$\theta'' = \frac{\rho A d}{2I} C_m(\theta) + \theta' \frac{\rho A}{2m} C_D$$

multiplying both sides by θ' , and ignoring the last term

$$\frac{\theta' d\theta'}{dX} = \frac{\rho A d}{2I} C_m(\theta) \frac{d\theta}{dX}$$

Integrating from θ_0 to θ , and noting that at θ_0 , $\theta' = 0$, we have

$$\theta' = \pm \left[\frac{\rho A d}{I} \int_{\theta_0}^{\theta} C_m(\theta) d\theta \right]^{1/2} \quad (4)$$

where the sign of θ' is dependent upon the sign of θ_0 . Using this expression for the angular velocity, a solution for the dynamic stability coefficient of an axisymmetric body with general lift and drag curves at any oscillation amplitude will be developed for a linear pitching moment case. In addition, characteristics of the nonlinear problem and a specific nonlinear pitching-moment curve will be discussed.

a. Linear pitching moment. $C_m(\alpha) = C_{m_\alpha} \alpha$

$$\begin{aligned} \theta' &= \pm \left[\frac{\rho A d}{I} \int_{\theta_0}^{\theta} C_{m_\alpha} \theta d\theta \right]^{1/2} \\ &= \pm \left[\left(-C_{m_\alpha} \frac{\rho A d}{2I} \right)^{1/2} (\theta_0^2 - \theta^2)^{1/2} \right] \end{aligned}$$

Arbitrary lift and drag curves may be approximated to any desired accuracy by power series in θ . Since the body is axisymmetric, the two series will be odd and even, respectively.

$$\begin{aligned} C_L(\theta) &= C_{L_\alpha} \theta + \sum_{i=1}^m b_i \theta^{2i+1} \\ C_D(\theta) &= C_{D_0} + \sum_{i=1}^n c_i \theta^{2i} \end{aligned}$$

Inserting these series in the energy equation (Eq. 3) and performing the indicated integrations yield the following solution for a half cycle:

$$\{C_{m_q} + C_{m_\alpha}\} \frac{m d^2}{I} = \frac{-4m}{\rho A} \frac{\Omega}{\pi} \frac{\delta \theta}{\theta_0} + \left[C_{L_\alpha} + 2 \sum_{i=1}^m \left(\prod_{j=1}^{i+1} \frac{2j-1}{2j} \right) b_i \theta_0^{2i} \right] - \left[C_{D_0} + 2 \sum_{i=1}^n \frac{1}{2(i+1)} \left(\prod_{j=1}^i \frac{2j-1}{2j} \right) c_i \theta_0^{2i} \right]$$

Notice that the above solution is equivalent to the solution of the linear differential equation when the b_i and c_i are set equal to 0 and the excellent approximation $-\ln(\alpha_x/\alpha_0) = \delta\theta/\theta_0$ is employed. By extension then, this solution provides a correction to the linear solution which will account for nonlinear lift and drag over an arbitrary number of cycles. However, the corrections are based on an amplitude value which changes during the flight due to the decay. It is therefore necessary to define a new amplitude value to be used for calculations and data correlation. The mean square resultant angle-of-attack δ^2 is defined as

$$\delta^2 = \int_0^X \alpha^2 dX / X$$

For a constant decay which is small in comparison with the oscillatory frequency

$$\delta^2 = \frac{\alpha_x^2 - \alpha_0^2}{4 \ln \left(\frac{\alpha_x}{\alpha_0} \right)}$$

The mean amplitude for the flight $\bar{\alpha}_0$ will be defined in terms of δ^2 :

$$\bar{\alpha}_0^2 \equiv 2\delta^2 = \frac{\alpha_x^2 - \alpha_0^2}{2 \ln \left(\frac{\alpha_x}{\alpha_0} \right)}$$

In the limit as the decay approaches zero, $\bar{\alpha}_0 = \alpha_0$. In the same manner that δ^2 best represents the mean square angle-of-attack, $\bar{\alpha}_0$ best represents the mean amplitude.

The useable solution for the dynamic stability coefficient for a body with a linear pitching moment is then

$$\begin{aligned} &\{C_{m_q} + C_{m_\alpha}\} \frac{m d^2}{I} \\ &= \frac{4m}{\rho A} \frac{1}{X - X_0} \ln \left(\frac{\alpha_x}{\alpha_0} \right) \\ &+ \left(C_{L_\alpha} + 2 \sum_{i=1}^m \left(\prod_{j=1}^{i+1} \frac{2j-1}{2j} \right) b_i \bar{\alpha}_0^{2i} \right) \\ &- \left(C_{D_0} + 2 \sum_{i=1}^n \frac{1}{2(i+1)} \left(\prod_{j=1}^i \frac{2j-1}{2j} \right) c_i \bar{\alpha}_0^{2i} \right) \end{aligned} \quad (5)$$

As an example of the lift and drag correction factors, if lift and drag are given by the expressions

$$C_L = C_{L_0}\theta + b_1\theta^3 + b_2\theta^5; \quad C_D = C_{D_0} + c_1\theta^2 + c_2\theta^4$$

the lift and drag terms in the solution are, respectively,

$$C_{L_\alpha} + \frac{3}{4}b_1\bar{\alpha}_0^2 + \frac{5}{8}b_2\bar{\alpha}_0^4 \quad \text{and} \quad C_{D_0} + \frac{c_1}{4}\bar{\alpha}_0^2 + \frac{c_2}{8}\bar{\alpha}_0^4$$

The applicability of this solution for several lift and drag curves has been verified with an exact computer solution of the equations of motion. The analytical forms of the aerodynamic coefficients were entered into the program and the resulting motion computed. $\{C_{m_q} + C_{m_{\dot{\alpha}}}\}$ was then calculated with the above solution using the computer decay. The deviation between the result and the input value of $\{C_{m_q} + C_{m_{\dot{\alpha}}}\}$ was less than 1% in all cases. Figure 8 shows a representative envelope calculated with this solution compared to an envelope calculated with the six-degree-of-freedom program.

b. Nonlinear pitching moments. Nonlinear pitching moments which can be represented by a power series or trigonometric functions add a substantial complication to the problem. A first integration yielding an expression for θ' may still be performed. However, further integrations such as those involved in Eq. (3) generally lead to elliptic integrals of the first and second types. Therefore, a closed form solution for a general pitching moment cannot be obtained. Given a body exhibiting a particular nonlinear moment, two possible approaches to the data reduction problem are (1) define an effective constant pitching moment slope $C_{m_{\alpha_{\text{eff}}}}$ which will give the same distance period of oscillation over a quarter cycle as does the nonlinear moment, and use the linear solution with this effective coefficient; $C_{m_{\alpha_{\text{eff}}}}$ will, of course, vary with oscillation amplitude; and (2) actually set up and integrate the elliptic integrals involved using the nonlinear moment. The second choice may involve a great deal of work and, in some cases, might not even be possible. Furthermore, the solution will not be in a form which is easily useable for parametric studies. However, in the first approach, though the distance oscillation period is matched, θ upon which the static aerodynamics are dependent and θ' upon which the damping moment is dependent may vary greatly over a quarter oscillation cycle between the linear and the nonlinear cases. Thus, a significant loss of accuracy might occur if the first approach is employed. In general then, the characteristics

of any particular nonlinear moment must be examined, and perhaps the first, the second, or some combination of these two approaches may be employed.

For illustrative purposes, a pitching moment of the form $C_m(\alpha) = C_{m_\alpha}\alpha + 2r_m\alpha^3$ where $r_m > 0$ (destabilizing) will be analyzed. As a basis of analysis, the equation of motion neglecting all terms except the pitching moment will be solved completely for both a linear and a cubic pitching moment. By equating distance oscillation frequencies over a quarter cycle, the effect of the nonlinear moment on θ and θ' may be determined. This will lead the way to a solution for the complete nonlinear equation and to a derivation of a correction factor which will account for the effects of the nonlinear moment when applied to the linear solution. The equation to be solved is then,

$$I\theta'' = \frac{1}{2}\rho Ad C_m(\theta)$$

$$\text{Linear case. } C_m(\theta) = C_{m_{\alpha_{\text{eff}}}}\theta$$

$$\theta'_l = \pm \left(-C_{m_{\alpha_{\text{eff}}}} \frac{\rho Ad}{2I} \right)^{1/2} (\theta_0^2 - \theta^2)^{1/2}$$

If the body started at an initial angle $-\theta_0$, the sign of θ' will be positive over the first half cycle. Defining the distance $X = 0$ when the model passes through $\theta = 0$, a second integration yields distance as a function of θ over a quarter cycle:

$$X_l = \left(\frac{1}{-C_{m_{\alpha_{\text{eff}}}} \frac{\rho Ad}{2I}} \right)^{1/2} \int_0^{\theta} \frac{d\theta}{(\theta_0^2 - \theta^2)^{1/2}} \\ = \left(\frac{1}{-C_{m_{\alpha_{\text{eff}}}} \frac{\rho Ad}{2I}} \right)^{1/2} \sin^{-1} \frac{\theta}{\theta_0}$$

$$\text{Cubic case. } C_m(\theta) = C_{m_\alpha}\theta + 2r_m\theta^3 \text{ (see Fig. 9)}$$

$$\theta'_n = \pm \left(\frac{\rho Ad}{2I} \right)^{1/2} [-C_{m_\alpha}(\theta_0^2 - \theta^2) - r_m(\theta_0^4 - \theta^4)]^{1/2}$$

$$X_n = \left(\frac{1}{r_m \frac{\rho Ad}{2I}} \right)^{1/2} \int_0^{\theta} \frac{d\theta}{(\theta^2 - \theta_0^2)^{1/2} \left(\theta^2 + \frac{C_{m_\alpha}}{r_m} + \theta_0^2 \right)^{1/2}}$$

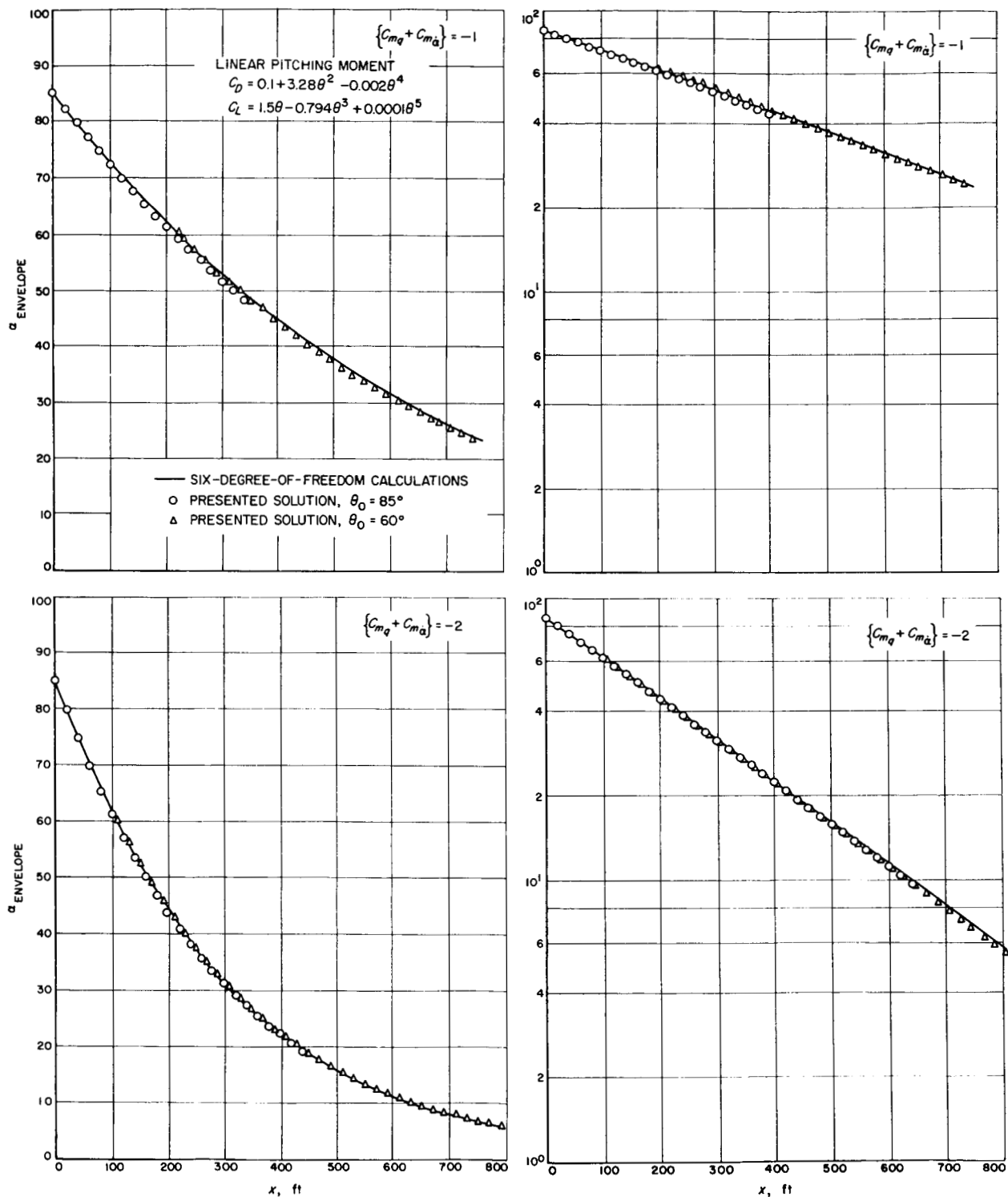


Fig. 8. Comparison of linear-solution envelope to six-degree-of-freedom envelope

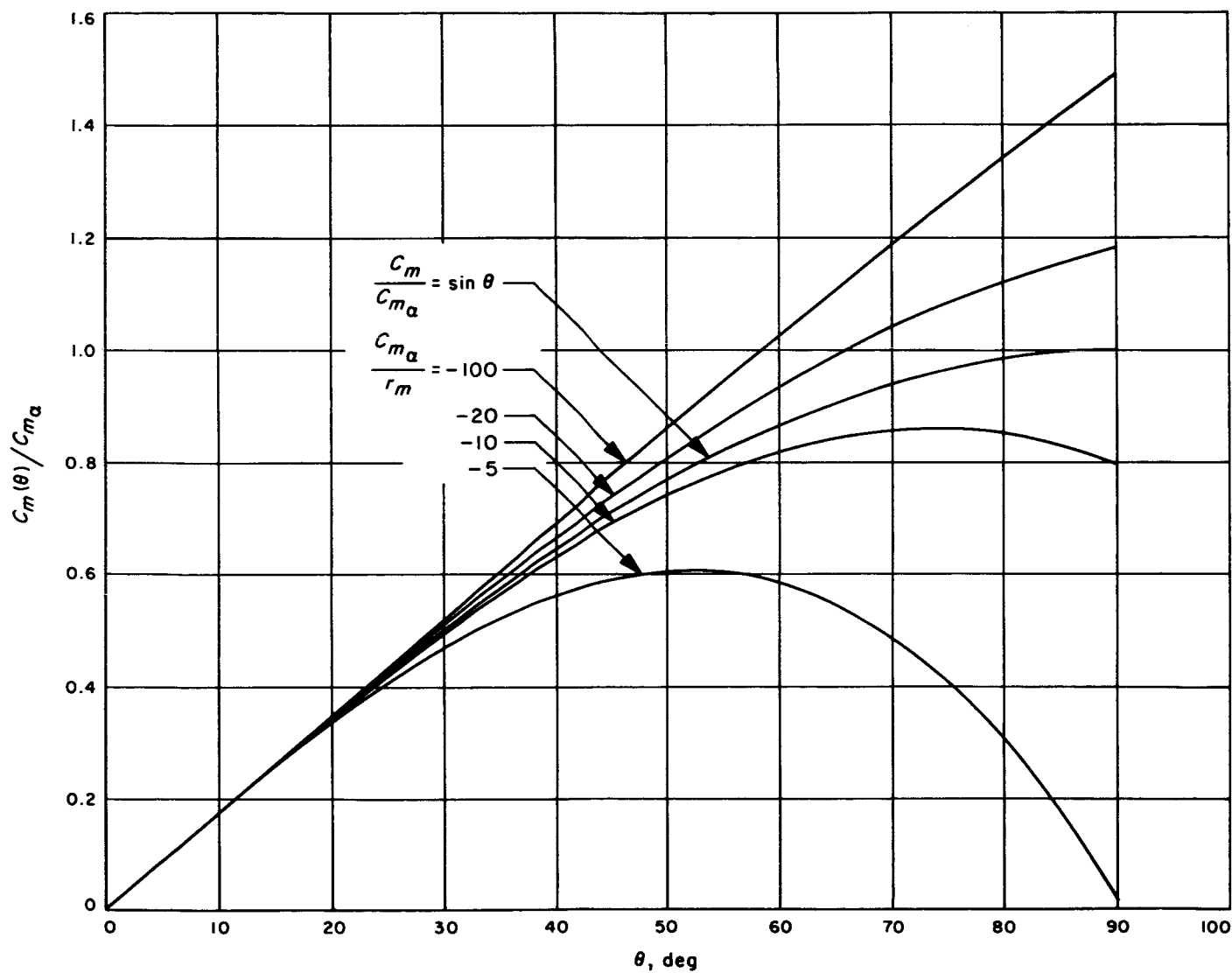


Fig. 9. Representative cubic pitching moments

Note that if the body is statically stable at $\theta_0 > 0$, then $C_{m_\alpha}\theta_0 + 2r_m\theta_0^3 < 0$ and therefore the following three inequalities hold:

$$\frac{C_{m_\alpha}}{2r_m} + \theta_0^2 < 0; \frac{C_{m_\alpha}}{r_m} + \theta_0^2 < 0; -\frac{C_{m_\alpha}}{r_m} > 2\theta_0^2$$

Let $-q^2 = (C_{m_\alpha}/r_m) + \theta_0^2$. Then $q^2 > \theta_0^2$ and

$$X_n = \left(\frac{1}{r_m}\right)^{1/2} \left(\frac{2I}{\rho A d}\right)^{1/2} \int_0^{\theta_0} \frac{d\theta}{(\theta^2 - \theta_0^2)^{1/2} (\theta^2 - q^2)^{1/2}}$$

Employing the substitutions $k^2 = \theta_0^2/q^2 < 1$ and $\phi = \sin^{-1} \theta/\theta_0$,

$$\begin{aligned} X_n &= \frac{1}{q} \left(\frac{1}{r_m}\right)^{1/2} \left(\frac{2I}{\rho A d}\right)^{1/2} \int_0^\phi \frac{d\phi}{(1 - k^2 \sin^2 \phi)^{1/2}} \\ &= \left(\frac{-1}{C_{m_\alpha} + r_m\theta_0^2}\right)^{1/2} \left(\frac{2I}{\rho A d}\right)^{1/2} F(k, \phi) \end{aligned}$$

where $F(k, \phi)$ is the Legendre canonical form of an elliptic integral of the first kind (Ref. 4). Figure 10 relates k^2 to C_{m_α}/r_m and θ_0 . An expression for an effective linear

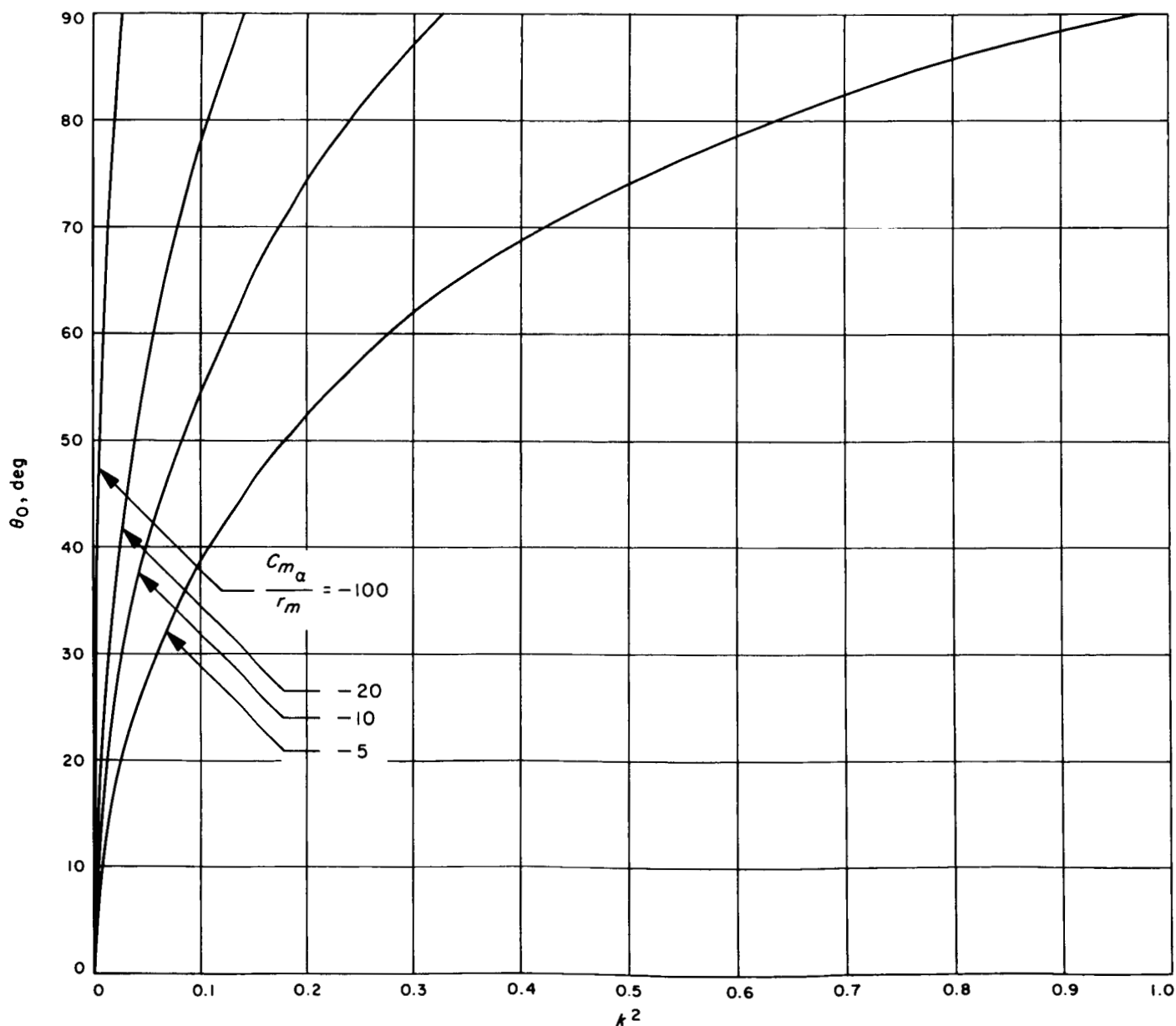


Fig. 10. k^2 vs θ_0 for various values of parameter C_{m_α}/r_m

pitching moment slope which yields the same distance period of oscillation over a quarter cycle as does the non-linear moment may now be derived by equating the expressions for X_l and X_n .

$$\frac{X_l}{X_n} = 1 = \frac{\left(\frac{-2I}{\rho A d C_{m_{\alpha_{\text{eff}}}}}\right)^{1/2} \frac{\pi}{2}}{\left(\frac{-1}{C_{m_{\alpha}} + r_m \theta_0^2}\right)^{1/2} \left(\frac{2I}{\rho A d}\right) F(k, \pi/2)}$$

$$C_{m_{\alpha_{\text{eff}}}} = \frac{(C_{m_{\alpha}} + r_m \theta_0^2) \pi^2 / 4}{[F(k, \pi/2)]^2}$$

of experimental data. $C_{m_{\alpha_{\text{eff}}}}$ may be calculated for several oscillation amplitudes (as many as possible) from the experimental frequency using the linear solution. Then $C_{m_{\alpha}}$ and r_m may be obtained through a least squares curve fit of the $C_{m_{\alpha_{\text{eff}}}}$ vs θ_0 data. A derivation of the least-squares equations for this fit are presented in Appendix B.

Assuming that locally θ_n is a slight perturbation of θ_l , the following approximate angle ratio can be written:

$$\frac{\theta_l}{\theta_n} \approx \frac{\sin \Omega X_l}{\sin \Omega X_n} = \frac{\sin \theta_l}{\sin \left(\theta_l \frac{X_n}{X_l} \right)}$$

where

$$\frac{X_n}{X_l} = \left(\frac{C_{m_{\alpha_{\text{eff}}}}}{C_{m_{\alpha}} + r_m \theta_0^2} \right)^{1/2} \frac{F(k, \phi)}{\phi}$$

Figure 11 shows $C_{m_{\alpha_{\text{eff}}}}$ as a function of θ_0 calculated from several hypothetical cubic pitching-moment curves. Since the oscillation frequency is a function primarily of the pitching moment, Eq. (6) provides a method to obtain the coefficients of a cubic pitching moment from a set

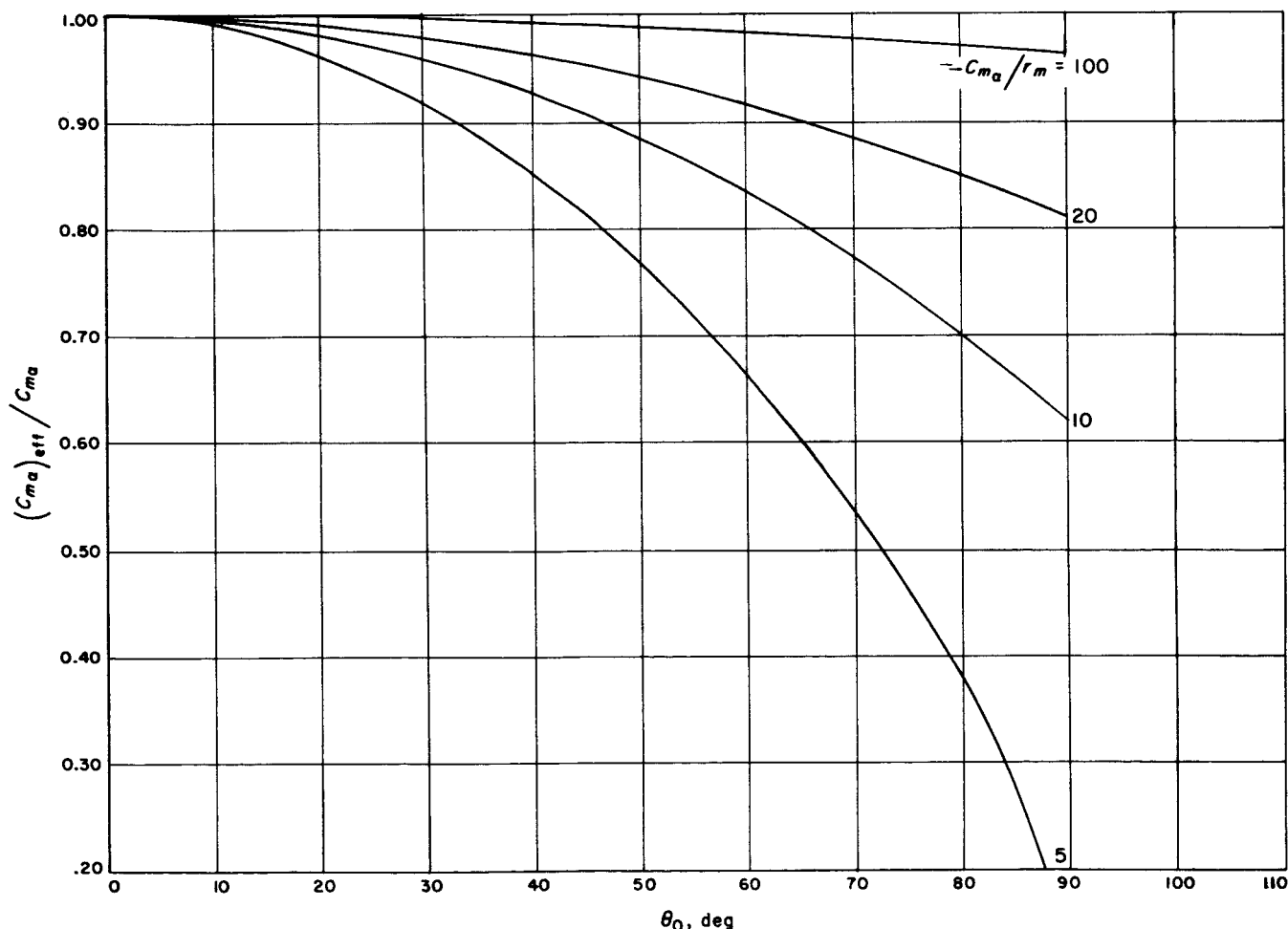


Fig. 11. $C_{m_{\alpha_{\text{eff}}}}$ vs θ_0 for various values of parameter $C_{m_{\alpha}}/r_m$

and substituting for $C_{m_{\alpha_{eff}}}$,

$$\frac{X_n}{X_l} = \frac{\pi/2}{F(k, \pi/2)} \frac{F(k, \phi)}{\phi}$$

Since

$$k^2 = \frac{-\theta_0^2}{C_{m_\alpha}/r_m + \theta_0^2}$$

and $\phi = \sin^{-1} \theta/\theta_0$, it can be seen that the distance ratio and angle ratio are both functions of only θ_0 , θ and C_{m_α}/r_m , and independent of the actual magnitude of the cubic coefficients. θ_l/θ_n and X_n/X_l are plotted in Figs. 12 and 13 for various values of the ratio C_{m_α}/r_m .

Similarly the ratio θ'_l/θ'_n may be formed:

$$\frac{\theta'_l}{\theta'_n} = \left(\frac{C_{m_{\alpha_{eff}}} (\theta_0^2 - \theta^2)}{r_m (\theta_0^2 - \theta^2) \left(\theta^2 + \frac{C_{m_\alpha}}{r_m} + \theta_0^2 \right)} \right)^{1/2}$$

Substituting for $C_{m_{\alpha_{eff}}}$, and for $\theta \neq \theta_0$

$$\frac{\theta'_l}{\theta'_n} = \left(\frac{\frac{C_{m_\alpha}}{r_m} + \theta_0^2}{\frac{C_{m_\alpha}}{r_m} + \theta_0^2 + \theta^2} \right)^{1/2} \frac{\pi/2}{F(k, \pi/2)}$$

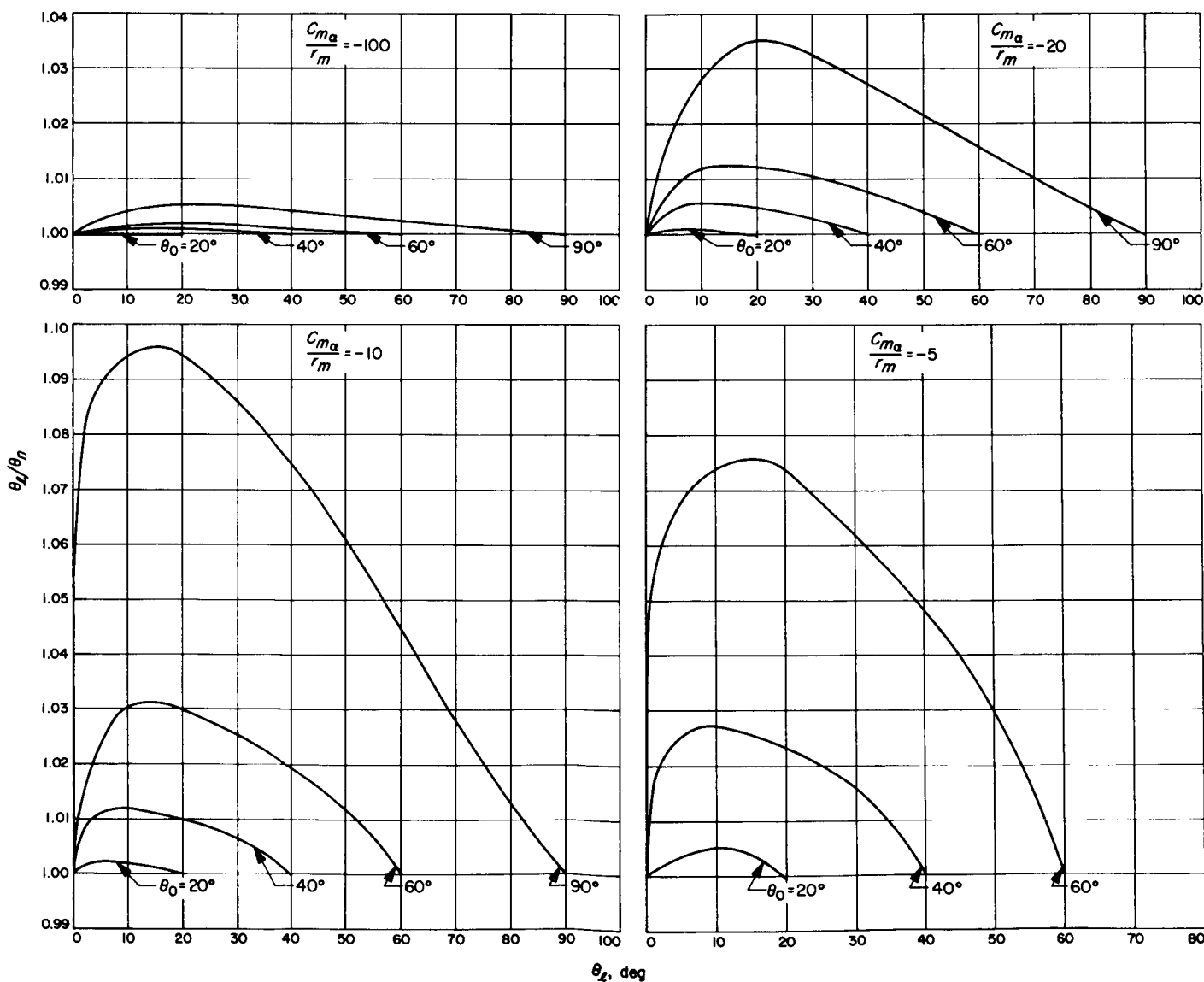
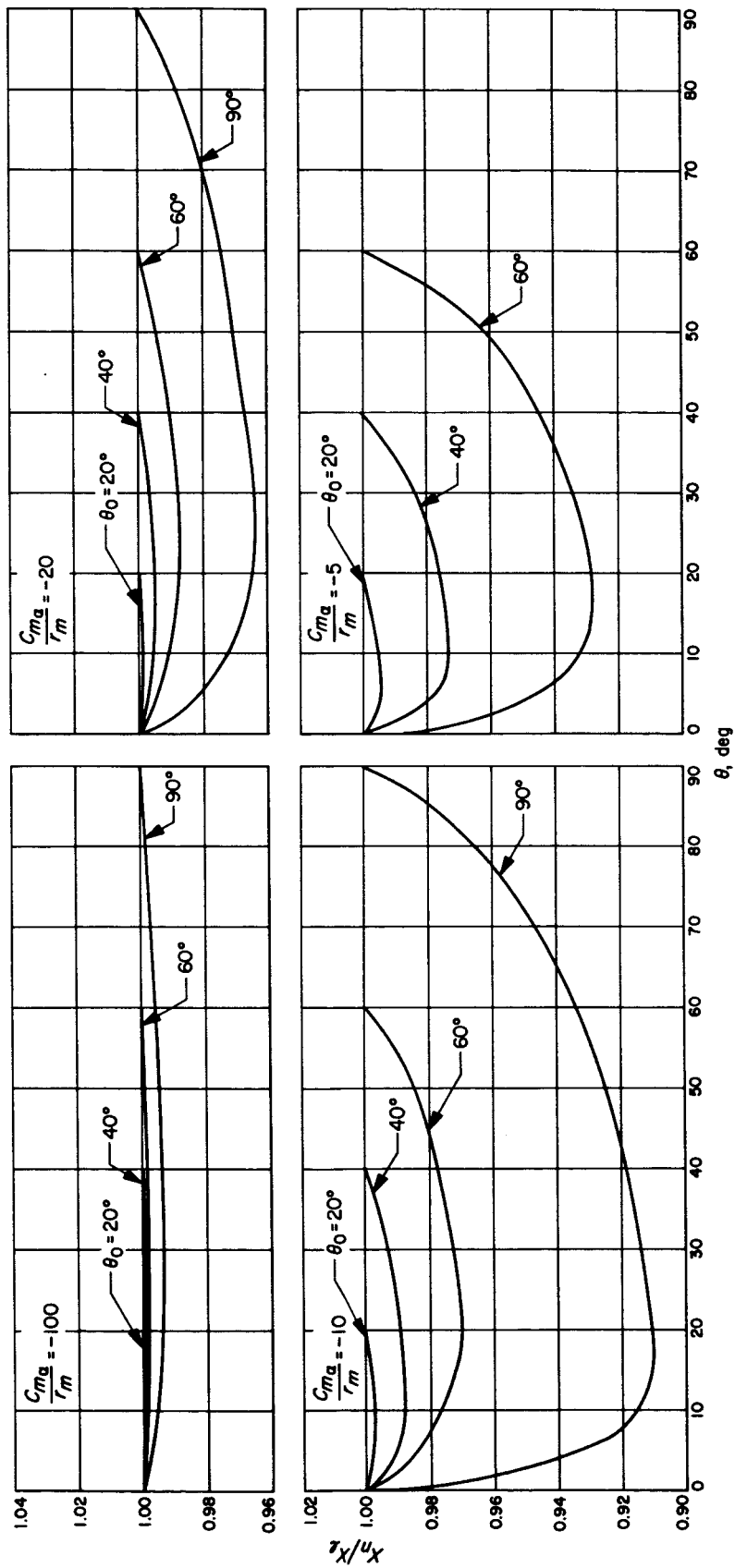


Fig. 12. θ_l/θ_n vs θ_l for various values of parameter C_{m_α}/r_m

Fig. 13. X_n/X_l vs θ for various values of parameter C_{ma}/r_m

Again, this is independent of the absolute values of C_{m_α} and r_m , but is a function of θ , θ_0 , and C_{m_α}/r_m . Figures 14 and 15 are parametric representations of this ratio.

Perhaps of more interest than the θ' ratio is the ratio of the integrals of the angular velocities over a half oscillation cycle since these integrals represent weighing factors with regard to the effects of $\{C_{m_q} + C_{m_\alpha}\}$.

$$\frac{\int_{-\theta_0}^{\theta_0} \theta'_i d\theta}{\int_{-\theta_0}^{\theta_0} \theta'_n d\theta} = \frac{(-C_{m_{\alpha_{eff}}})^{1/2} \int_{-\theta_0}^{\theta_0} (\theta_0^2 - \theta^2)^{1/2} d\theta}{(r_m)^{1/2} \int_{-\theta_0}^{\theta_0} (\theta^2 - \theta_0^2)^{1/2} \left(\theta^2 + \frac{C_{m_\alpha}}{r_m} + \theta_0^2 \right)^{1/2} d\theta}$$

The denominator involves elliptic integrals of both the first and the second types. The following equality can be shown:

$$\int_{-\theta_0}^{\theta_0} (\theta^2 - \theta_0^2)^{1/2} \left(\theta^2 + \frac{C_{m_\alpha}}{r_m} + \theta_0^2 \right)^{1/2} d\theta = \frac{2}{3} \times \left[- \left(\frac{C_{m_\alpha}}{r_m} + \theta_0^2 \right)^{3/2} [(1 + k^2) E(k, \pi/2) - \bar{k}^2 F(k, \pi/2)] \right]$$

where again

$$k^2 = \frac{-\theta_0^2}{\frac{C_{m_\alpha}}{r_m} + \theta_0^2},$$

$\bar{k}^2 = 1 - k^2$, and F and E are the Legendre canonical forms of elliptic integrals of the first and second kinds, respectively. The ratio now becomes,

$$\frac{\int_{-\theta_0}^{\theta_0} \theta'_i d\theta}{\int_{-\theta_0}^{\theta_0} \theta'_n d\theta} = \frac{3}{2} \frac{-\theta_0^2}{\frac{C_{m_\alpha}}{r_m} + \theta_0^2} \frac{\pi^2/4}{F(k, \pi/2)}$$

$$\times \frac{1}{[(1 + k^2) E(k, \pi/2) - \bar{k}^2 F(k, \pi/2)]}$$

$$= \frac{3}{2} \frac{k^2 \pi^2/4}{F(k, \pi/2)} \frac{1}{[(1 + k^2) E(k, \pi/2) - \bar{k}^2 F(k, \pi/2)]}$$

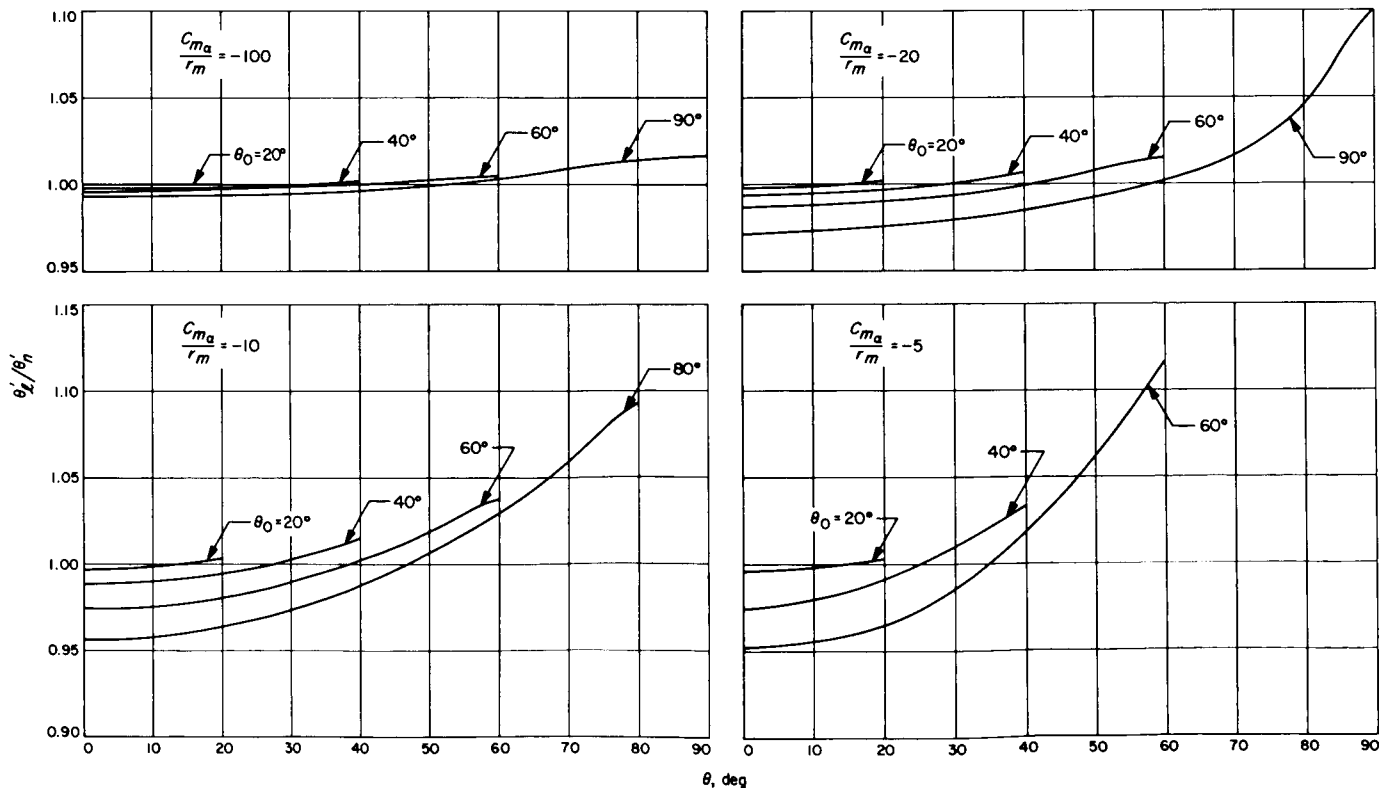


Fig. 14. θ'_i/θ'_n vs θ for various values of parameter C_{m_α}/r_m

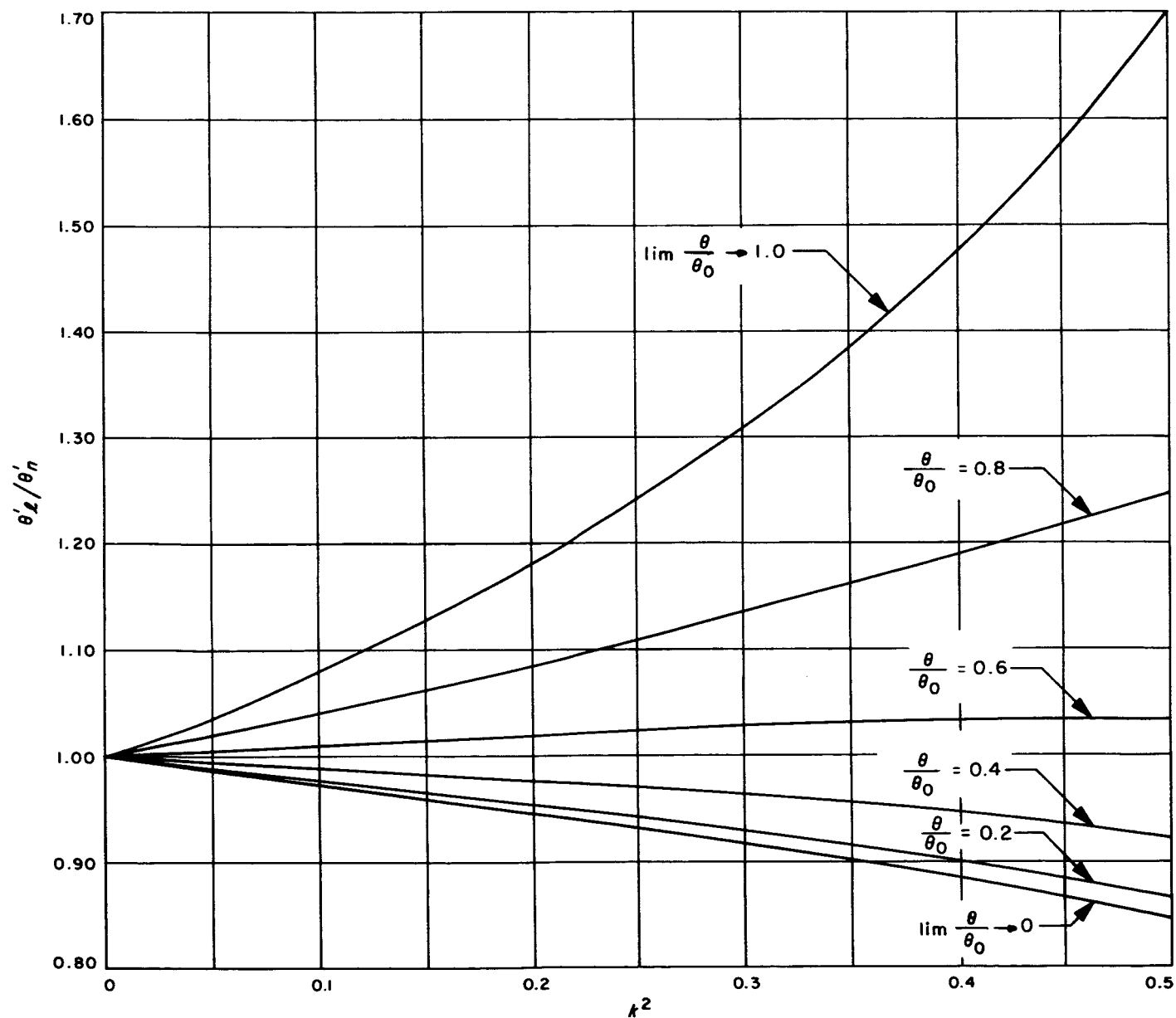


Fig. 15. θ'_L/θ'_n vs k^2 as a function of θ/θ_0

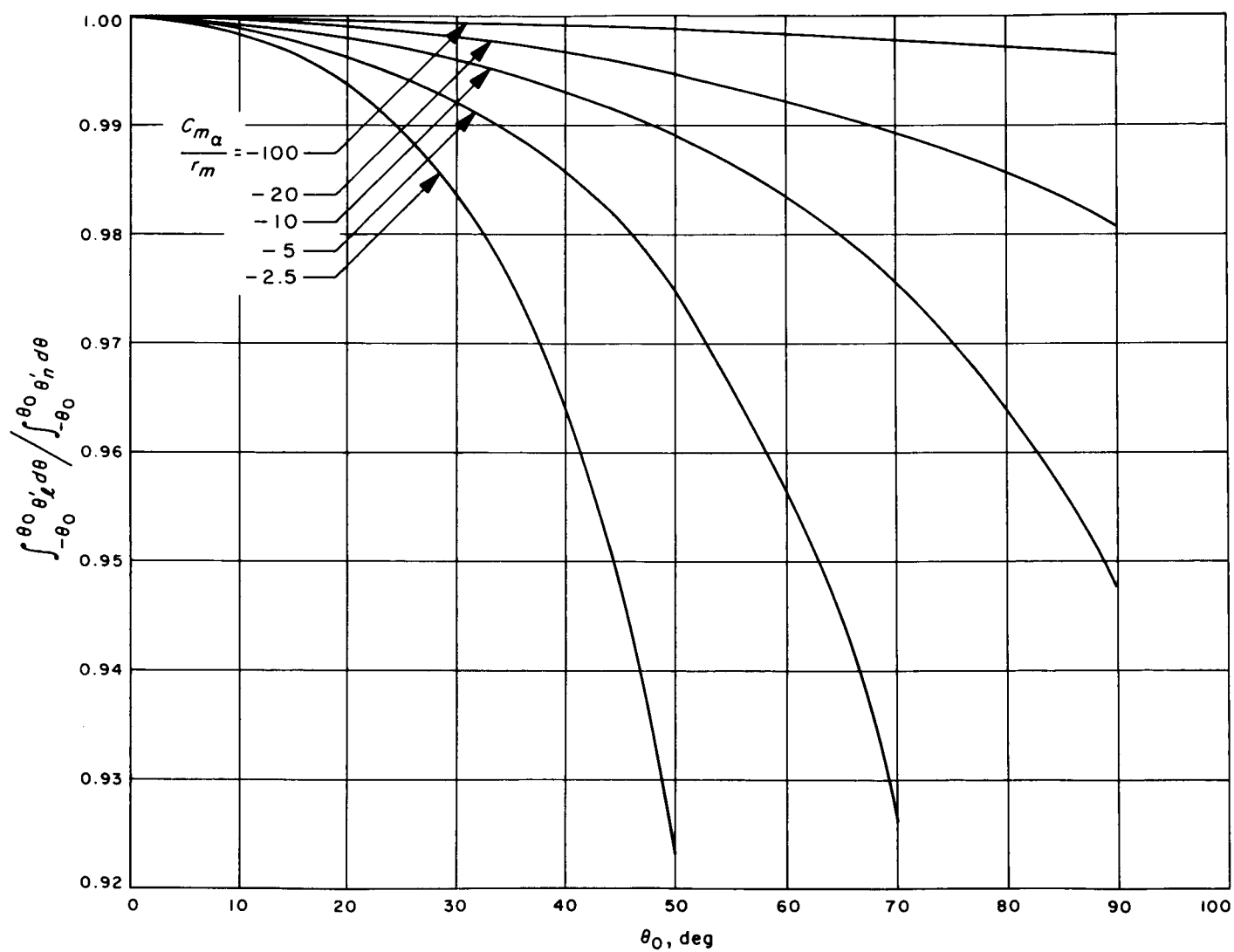


Fig. 16. $\int \theta'_t d\theta / \int \theta'_n d\theta$ vs θ_0 for various values of parameter C_{m_α}/r_m

This ratio is plotted vs θ_0 for several values of C_{m_α}/r_m in Fig. 16 and vs k^2 in Fig. 17.

These ratios actually represent the errors that would result if a body with a cubic pitching moment were analyzed with an effective linear moment. The difference between the nonlinear and linear angles would have to be used in conjunction with curves of the lift and drag coefficients. The error in this dissipative term,

$$\{C_{m_q} + C_{m_\alpha}\} \int_{-\theta_0}^{\theta_0} \theta' d\theta$$

is available directly from Fig. 16.

With this development it is now possible to formulate an approach toward a solution for the damping coefficient. Figures 12 and 17, used in conjunction with the aerodynamics of the shape in question, would yield an assessment of errors introduced by employing a linear effective approximation. Each particular situation should be considered separately. However, a general practical approach would be to use linear effective aerodynamics for the

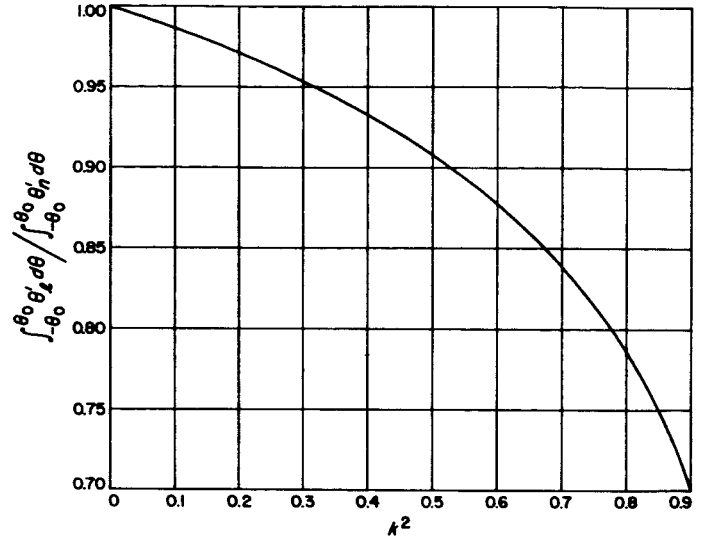


Fig. 17. $\int \theta'_l d\theta / \int \theta'_n d\theta$ vs k^2

second order terms, lift and drag, and the actual cubic pitching moment in the remaining terms. With this approach, integrating Eq. (3) and ignoring higher order terms of $\delta\theta$, the following solution results:

$$\begin{aligned} \{C_{m_q} + C_{m_\alpha}\} \frac{md^2}{I} = & \frac{\frac{3}{2} r_m \frac{md}{I} \theta_0 \delta\theta (C_{m_\alpha} + 2r_m \theta_0^2)}{\left(\frac{\rho A d}{2I}\right)^{1/2} [-(C_{m_\alpha} + r_m \theta_0^2)]^{1/2} [(1 + k^2) E(k, \pi/2) - \bar{k}^2 F(k, \pi/2)]} \\ & + \left(C_{L_\alpha} + 2 \sum_{i=1}^m \left(\prod_{j=1}^{i+1} \frac{2j-1}{2j}\right) b_i \theta_0^{2i}\right) - \left(C_{D_0} + 2 \sum_{i=1}^n \frac{1}{2(i+1)} \left(\prod_{j=1}^i \frac{2j-1}{2j}\right) c_i \theta_0^{2i}\right) \end{aligned}$$

This last equation may be put into a more useful form by writing the first term as a product of a linear solution term and the ratio of a nonlinear to linear term:

$$\begin{aligned} \frac{-md}{I} \frac{\left[\int_{-(\theta_0 - \delta\theta)}^{\theta_0} C_m(\theta) d\theta\right]_n}{\int_{-\theta_0}^{\theta_0} \theta'_n d\theta} &= \frac{-md}{I} \frac{\left[\int_{-(\theta_0 - \delta\theta)}^{\theta_0} C_m(\theta) d\theta\right]_l}{\int_{-\theta_0}^{\theta_0} \theta'_l d\theta} \frac{\left[\int_{-(\theta_0 - \delta\theta)}^{\theta_0} C_m(\theta) d\theta\right]_n}{\left[\int_{-(\theta_0 - \delta\theta)}^{\theta_0} C_m(\theta) d\theta\right]_l} \frac{\int_{-\theta_0}^{\theta_0} \theta'_l d\theta}{\int_{-\theta_0}^{\theta_0} \theta'_n d\theta} \\ &= \frac{-4m \Omega}{\rho A} \frac{\delta\theta}{\pi \theta_0} \frac{C_{m_\alpha} + 2r_m \theta_0^2}{C_{m_{\alpha_{eff}}}} \frac{\int_{-\theta_0}^{\theta_0} \theta'_l d\theta}{\int_{-\theta_0}^{\theta_0} \theta'_n d\theta} \\ &= \frac{-4m \Omega}{\rho A} \frac{\delta\theta}{\pi \theta_0} R \end{aligned} \quad (6)$$

where

$$R = \frac{\frac{3}{2} \bar{k}^2 k^2 F(k, \pi/2)}{[(1 + k^2) E(k, \pi/2) - \bar{k}^2 F(k, \pi/2)]}$$

The correction ratio R is plotted vs θ_0 for several values of C_{m_α}/r_m in Fig. 18 and k^2 in Fig. 19. Inserting this in the damping coefficient solution and extending over an arbitrary number of cycles in a manner similar to the linear case yield Eq. 7:

The applicability of this solution has also been checked with a six-degree-of-freedom program. Deviations between input and resultant values of $\{C_{m_q} + C_{m_{\dot{\alpha}}}\}$ were less than 3% in all cases, and less than 1% for the lower values of k^2 . Figure 20 shows envelope histories calculated with this solution as compared to envelopes calculated with the six-degree-of-freedom program for $C_{m_\alpha}/r_m = -20$.

$$\begin{aligned} \{C_{m_q} + C_{m_{\dot{\alpha}}}\} \frac{m d^2}{I} = & \left(\frac{4m}{\rho A} \right) \left(\frac{1}{X - X_0} \right) \ln \left(\frac{\alpha_x}{\alpha_0} \right) R + \left(C_{L_\alpha} + 2 \sum_{i=1}^m \left(\prod_{j=1}^{i+1} \frac{2j-1}{2j} \right) b_i \bar{\alpha}_0^{2i} \right) \\ & - \left(C_{D_0} + 2 \sum_{i=1}^n \frac{1}{2(i+1)} \left(\prod_{j=1}^i \frac{2j-1}{2j} \right) c_i \bar{\alpha}_0^{2i} \right) \end{aligned} \quad (7)$$

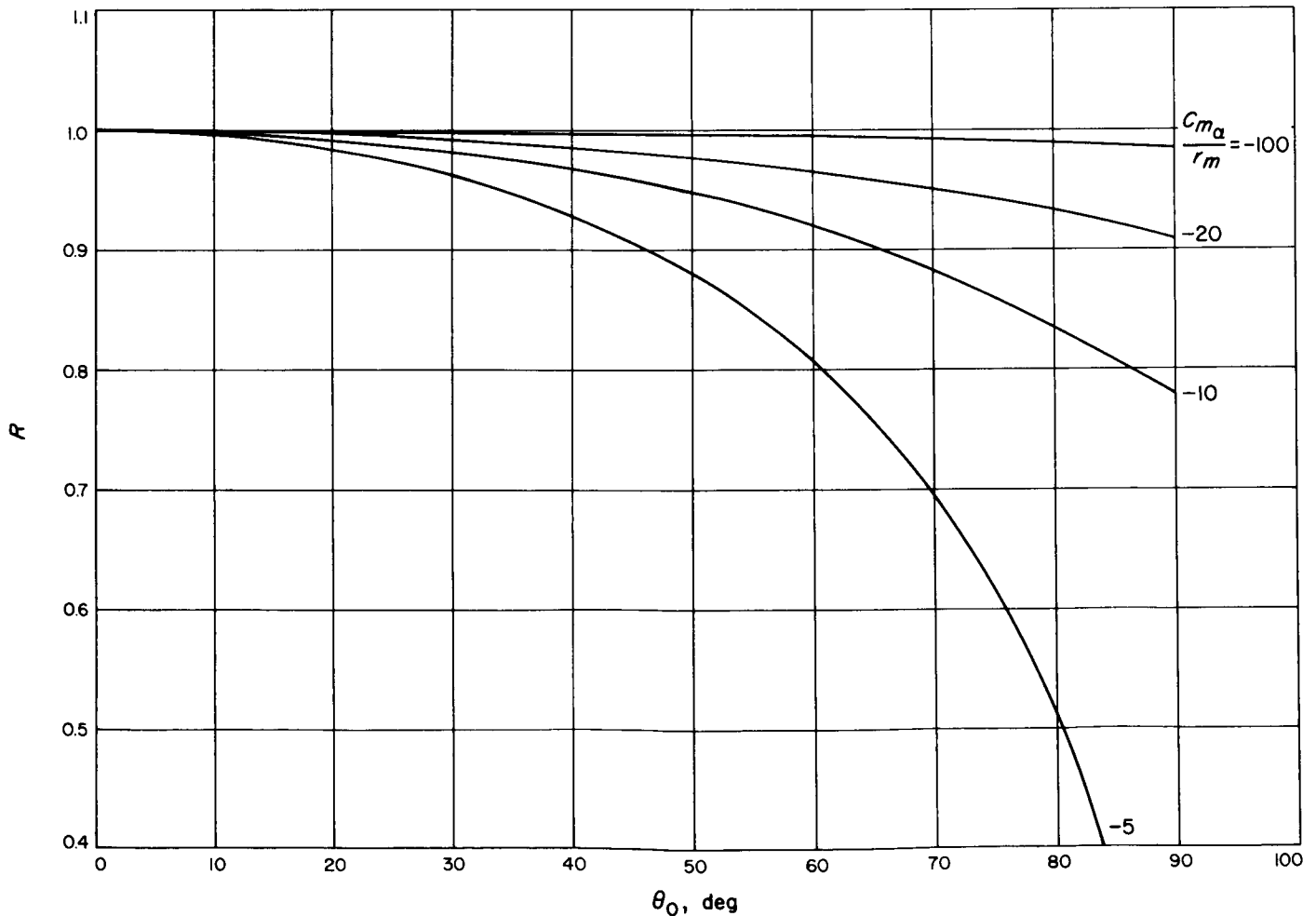


Fig. 18. Correction factor R vs θ_0 for various values of parameter C_{m_α}/r_m

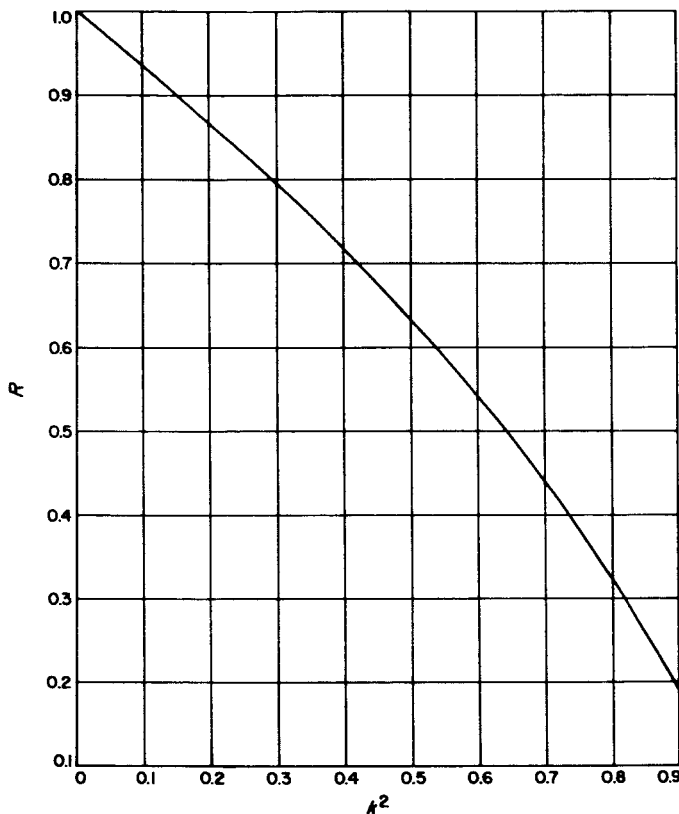


Fig. 19. Correction factor R vs k^2

E. Dynamic Stability Testing Capabilities

The free-flight technique has many capabilities for a large variety of wind-tunnel uses. Applications to dynamic stability testing alone show significant advantages over other testing techniques. The most prominent, of course, remains the various ramifications of support free data. The following discussion mentions some of the major benefits derived from this testing technique.

It is generally recognized that the presence of a sting, no matter how small, is likely to affect the base pressure and base heating of the test configuration. In turn, many

aerodynamic measurements, including dynamic stability, may be materially affected by the base flow conditions. However, usual evaluation from captive type tests tends towards the assumption that support interference is negligible. The free-flight technique offers a method to obtain support-free data which may be used to check the validity of this assumption.

In addition, the free-flight technique allows the extension of wind-tunnel dynamic stability testing into areas difficult or impossible to match with other techniques. Complete flexibility of initial angle of attack as well as the possibility of analyzing nonplanar motion are available. Experiments may be conducted in a high-oscillation frequency regime which cannot be matched in a captive free-oscillation test. The relatively low model accelerations allows great flexibility in the variation of such parameters as model size, center of gravity, and moment of inertia. Certainly, a much more meaningful base configuration study could be performed with this method than with any other technique.

From a qualitative point of view, the technique allows the experimenter an opportunity to see actual flight motion and corresponding stability trends. A rather important and useful by-product is the complete flow visualization record of the flight from the schlieren motion pictures.

The major limitation of the technique is the data reduction problem. Film reading is a costly and time consuming process, and, in general, is the primary limit on the amount of data to be reduced. The possibility of using accelerometers and a telemetry package to recreate the model motion could eliminate this problem. It would be feasible, under such a data acquisition technique, to have a completely automatic collecting and reduction system which would greatly reduce both time and cost. This, together with the extension to nonplanar motion, would seem to be the next step in technique development.

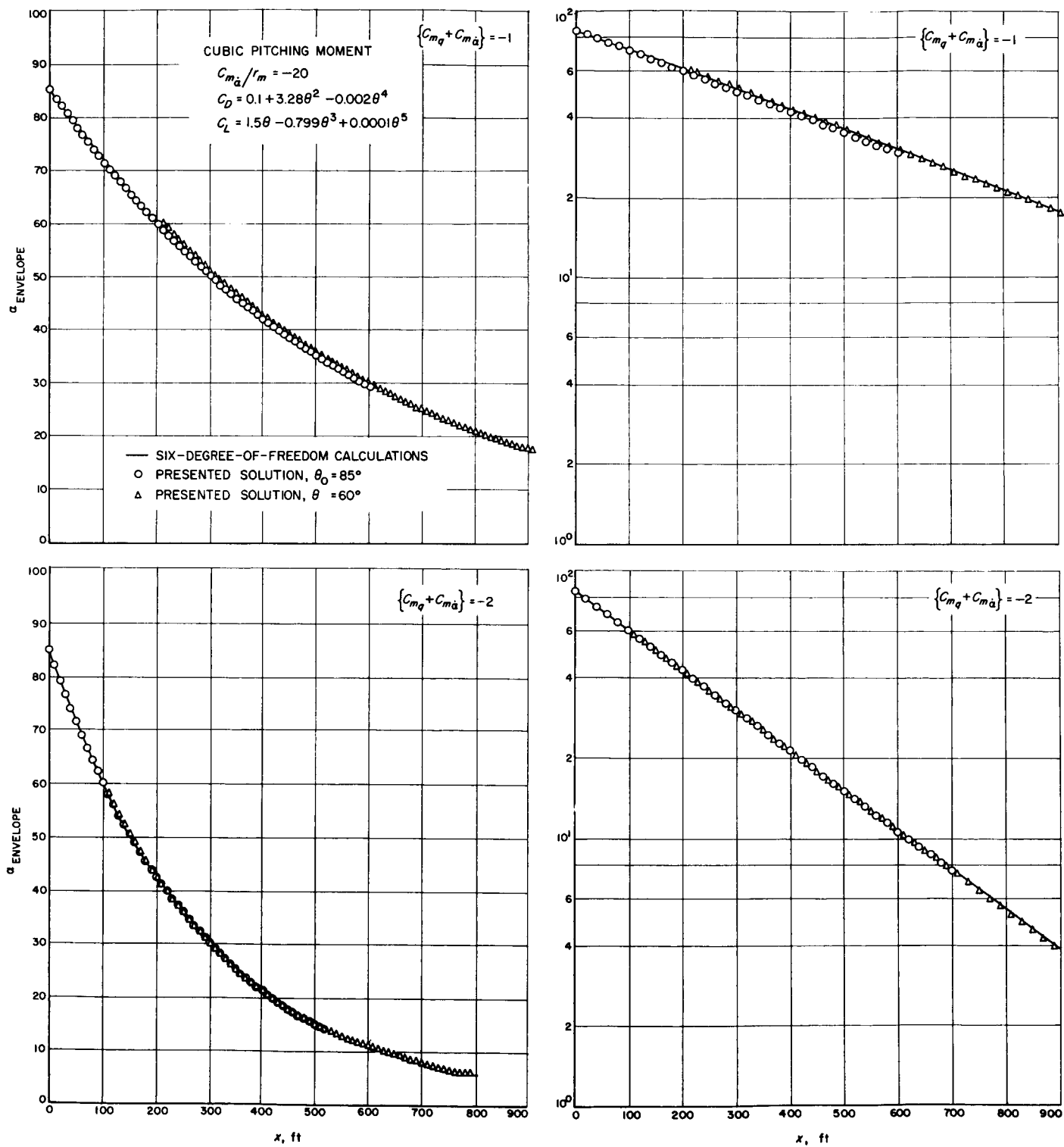


Fig. 20. Comparison of cubic-solution envelope to six-degree-of-freedom envelope

III. FREE-OSCILLATION TECHNIQUE

A. The Gas Bearing

The models are mounted in the wind tunnel at their center of gravity on a sting-supported low-friction gas bearing. High purity gaseous nitrogen at 200 psi is used as a lubricant. At this pressure, the bearing will support up to 55 lb of radial load. Exhaust gases are channeled to a point of release on the sting about 2 ft downstream of the model base. The bearing is 1-in. D, 2-in. long, and has a radial gap approximately 0.0005 in. (see Fig. 21). The maximum model angle of attack is limited by the sting and the model base to anywhere from 20 deg (sharp cone) to 45 deg (very blunt cone). The model may be remotely pitched to and released from the desired initial angle of attack.

The operation of the bearing is normally checked with a thin shell, low moment of inertia calibration sphere prior to the recording of any data. The sphere, mounted on a diameter, contains an offset mass to provide a restoring moment. It is pitched to its maximum angular excursion, released, and allowed to oscillate until damped by the bearing friction and the aerodynamics. Since the aerodynamic effects are small as the sphere oscillates about a diameter, this damping history provides a qualitative measure for the tare damping. Tunnel air flow provides loads of the same magnitude as those experienced by the test models, and yet the low moment of

inertia sphere maintains oscillation frequencies similar to that of a model. This is in contrast to a nonaerodynamic dead load calibration which would result in comparatively very low frequencies. The calibration sphere mounted on the bearing is shown in Fig. 22.

B. Data Acquisition

The data are collected through a system which uses an Optron Tracker,* a passive optical electronic device which is designed to follow the motion of an object without physical contact. A cutaway schematic is shown in Fig. 23. The tracker requires a target having a sharp delineation in brightness to provide contrast. This target is optically focused on a photo-cathode which emits an electron image toward and through an aperture into a photo-multiplier section. The photo-multiplier output is coupled to a differential amplifier which compares the output signal to a reference signal established with the sharp line of contrast centered on the aperture. Any deviation from this reference causes the differential amplifier output to become unbalanced and send a correction voltage to a deflection yoke. The deflection yoke re-positions the electron beam so it is again centered on the aperture, thus forming a complete servo loop. A readout voltage may be sampled from the differential amplifier output. If the target is not on the model center of rotation, angular deflection of the model will yield vertical displacement of the target, and the Optron Tracker output will be a function of model angle of attack. At 2-ft working distance, the tracker has a maximum displacement range of 0.8 in. with a resolution of 0.001 in. and a rise time of 50 μ sec. The instrument is calibrated statically by pitching the model to a known angle of attack and recording the output. The relationship between voltage output and model angle of attack is quite linear between -30 and $+30$ deg, thus minimizing the number of points necessary during a calibration.

The available output from the Optron Tracker is then a continuous analog record of the model angle of attack. All that is necessary in order to obtain dynamic stability is a record of the oscillation amplitude and frequency. Therefore, it is desirable to sample the Optron output only around peak angle-of-attack areas. This is accomplished as follows: zero voltage output, equivalent to zero angle of attack, is sensed electronically. Using this,

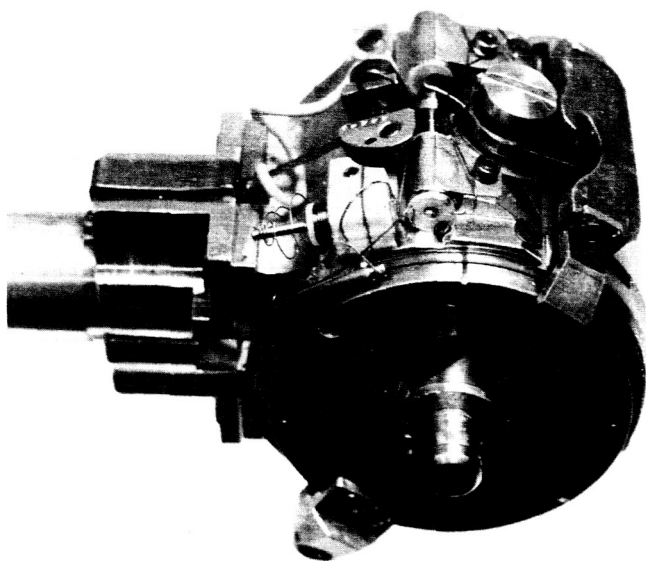


Fig. 21. The sting-supported gas bearing

*Manufactured by the Optron Corporation, Santa Barbara, Calif.

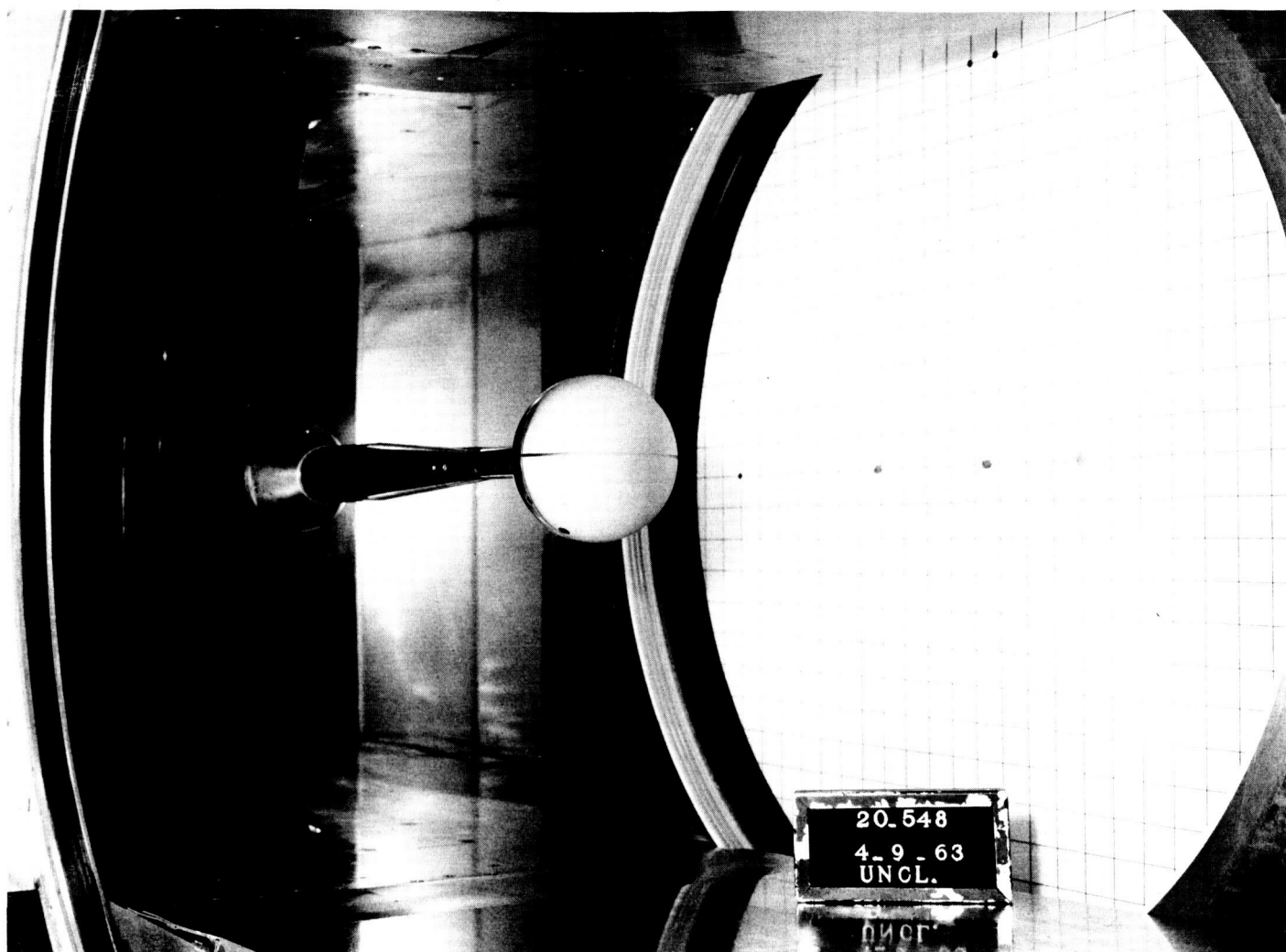


Fig. 22. Calibration sphere installation

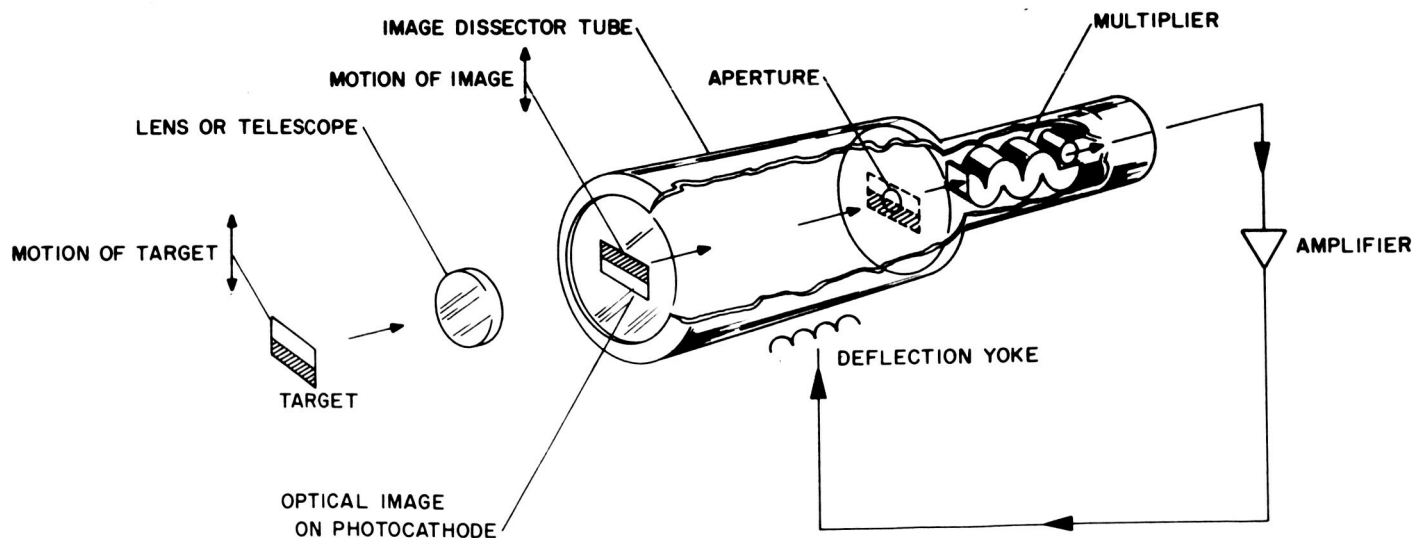


Fig. 23. Cutaway schematic of optron tracker

the period for each half oscillation cycle is measured and used to predict the occurrence of a peak two half cycles later (two to account for oscillation asymmetries). A sample of the Optron output is recorded 4.5 msec prior to the predicted peak time and every 0.5 msec thereafter until 4.5 msec after the predicted time (19 records). In general, this method will catch the peak, and in the cases where it does not, the 19 recorded points provide enough information to extrapolate the peak value. Applying a calibration and summing the half oscillation cycle times yield the raw data, a time vs oscillation amplitude history. The number of amplitude points per run varies between 30 for a high-damping, high-tunnel density run to as many as 1000 in the other extremes. Generally 3 or more runs are taken at each data point in order to provide a consistency check on both the equipment operation and the results. The angular position of the model can be determined to better than 0.2 deg. Part of this tolerance is due to difficulties in determining the actual angle of attack of the model during the calibration. The decay itself, upon which the dynamic stability coefficient is dependent, can be determined to about 0.1 deg. Figure 24 shows an amplitude vs time plot obtained through the free-oscillation techniques.

Because of the physical size of the bearing, the free oscillation models are necessarily large (4- to 5.25-in. D) in comparison to those used in the free-flight technique.

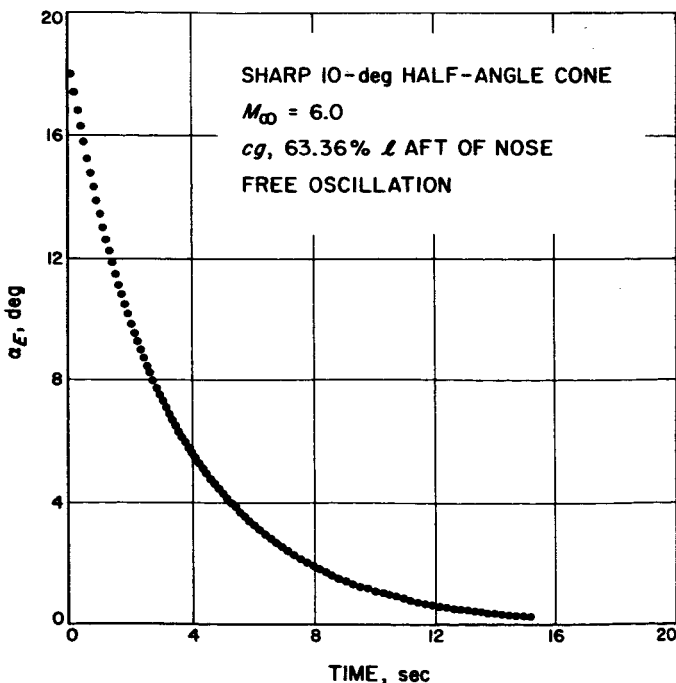


Fig. 24. Free-oscillation amplitude vs time

This, in turn, leads to substantial loads on the model and corresponding sting deflections as the model oscillates. In order to determine the effects, if any, of this sting motion on the model oscillatory history, the sting was instrumented with a strain gage bridge which provided a method to determine both loads and sting deflections. Output from the strain gage bridge is recorded simultaneously with the peak angular data, and in addition, recorded continuously with an oscillograph. Figure 25 presents an oscillograph trace showing the Optron Tracker output, the strain gage bridge output, and the triggering pulse corresponding to the initial scans of the 19 records around each peak. Notice that in this trace, no phase shift or higher harmonic motion is visible.

C. Data Reduction

The single-degree-of-freedom equation of motion for a body oscillating about a point is

$$I\ddot{\alpha} = C_m(\alpha) q_\infty A d + \{C_{m_q} + C_{m_{\dot{\alpha}}}\} \frac{q_\infty A d^2}{V_\infty} \dot{\alpha}$$

Two alternative cases for axisymmetric bodies will be considered: a linear pitching moment, and a cubic pitching moment. Because of the angle-of-attack limitations imposed by the hardware itself, one of these moment types generally provides a good approximation for most test configurations. In all instances $\{C_{m_q} + C_{m_{\dot{\alpha}}}\}$ will be an effective coefficient, assumed to remain constant over one oscillation cycle. The approach used will be parallel to that used in the free-flight case with the problem simplified in two respects. These are both due to the translational restraints imposed on the model and result in the velocity remaining constant and the condition $\alpha = \theta$. Neither lift nor drag terms will appear in the equations or solutions. Because of the similarity to the free-flight technique, derivations here will be brief, with many steps omitted.

1. Linear Pitching Moment ($C_m = C_{m_\alpha} \alpha$)

Again the solution is based on the premise that the pitching moment is the prime contributor to angular velocity. The solutions for the frequency and the envelope angle are

$$f = \frac{1}{2\pi} \left(-C_{m_\alpha} \frac{q_\infty A d}{I} \right)^{1/2}; \quad \alpha_t = \alpha_0 e^{\lambda t}$$

where $\lambda = \{C_{m_q} + C_{m_{\dot{\alpha}}}\} (q_\infty A d^2 / 2IV_\infty)$.

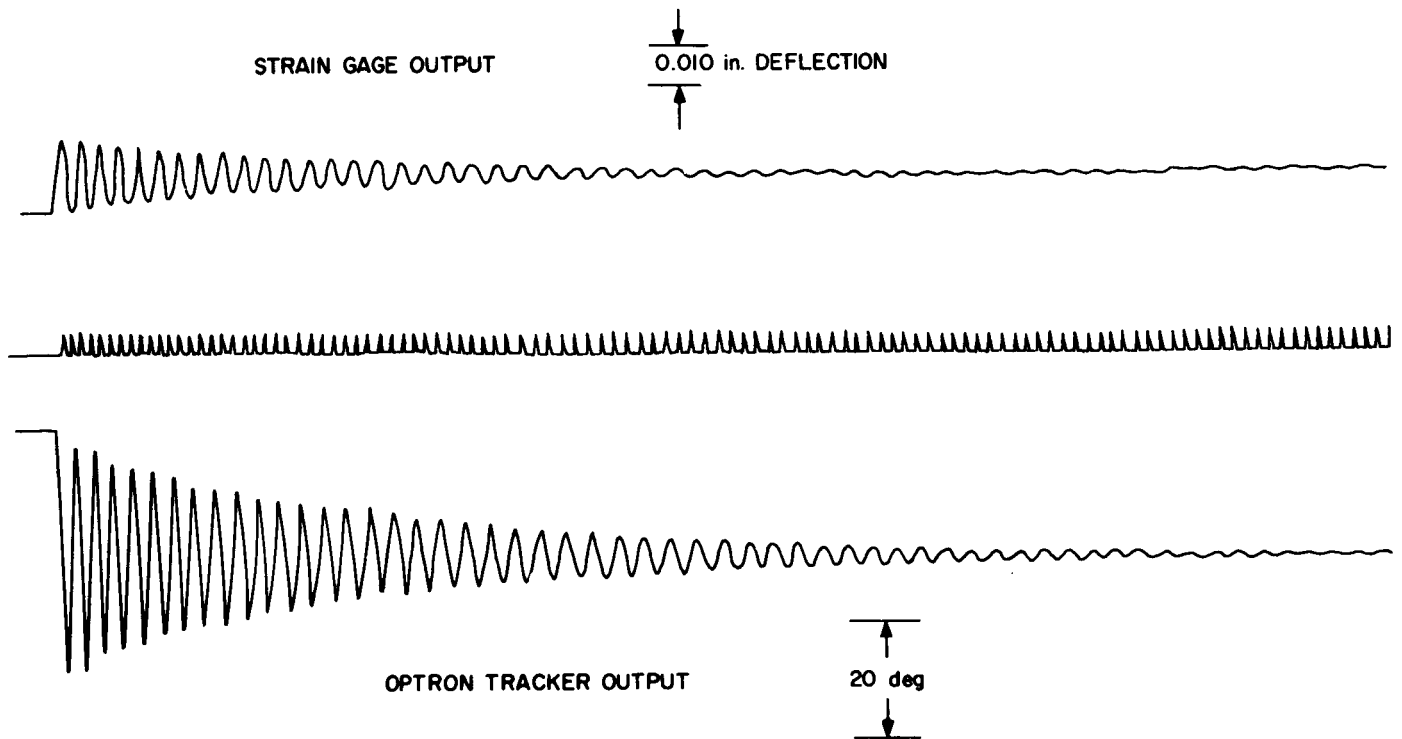


Fig. 25. Oscilloscope trace of optron and strain gage output

The corresponding solutions for the aerodynamic coefficients are

$$C_{m_\alpha} = \frac{-4\pi^2 f^2 I}{q_\infty A d}; \quad \{C_{m_q} + C_{m_{\dot{\alpha}}}\} = \frac{2IV_\infty}{q_\infty A d^2} \frac{1}{t} \ln \frac{\alpha_t}{\alpha_0}$$

2. Cubic Pitching moment ($C_m = C_{m_\alpha} \alpha + 2r_m \alpha^3$, $r_m > 0$)

The equation of motion becomes

$$I\ddot{\alpha} = (C_{m_\alpha} \alpha + 2r_m \alpha^3) q_\infty A d + \{C_{m_q} + C_{m_{\dot{\alpha}}}\} \frac{q_\infty A d^2}{V_\infty} \dot{\alpha}$$

Employing the assumption that the pitching velocity is a function of primarily the pitching moment, the following result is obtained:

$$\dot{\alpha} = \pm \left(\frac{q_\infty A d}{I} \right)^{1/2} [-C_{m_\alpha} (\alpha_0^2 - \alpha^2) - r_m (\alpha_0^4 - \alpha^4)]^{1/2}$$

An effective pitching moment slope which equates the oscillation frequencies between the linear and nonlinear case may be calculated from the experimental frequency using the linear solution. C_{m_α} and r_m are then obtained from a least-squares fit to the equation

$$C_{m_{\text{eff}}} = \frac{(C_{m_\alpha} + r_m \alpha_0^2) \pi^2 / 4}{[F(k, \pi/2)]^2}$$

where

$$k^2 = \frac{-\alpha_0^2}{\frac{C_{m_\alpha}}{r_m} + \alpha_0^2}$$

Using the above expression for α in the equation of motion yields the solution for $\{C_{m_q} + C_{m_{\dot{\alpha}}}\}$:

$$\{C_{m_q} + C_{m_{\dot{\alpha}}}\} = \frac{3}{2} \frac{r_m \alpha_0 \delta \alpha}{d} \left(\frac{2I}{\rho A d} \right)^{1/2} \frac{C_{m_\alpha} + 2r_m \alpha_0^2}{[-(C_{m_\alpha} + r_m \alpha_0^2)]^{3/2}} \frac{1}{[(1 + k^2) E(k, \pi/2) - k^2 F(k, \pi/2)]}$$

As in the free flight case, this may be written as the linear solution times a correction factor:

$$\{C_{m_q} + C_{m_{\dot{\alpha}}}\} = \frac{2IV_{\infty}}{q_{\infty}Ad^2} \frac{1}{t} \ln \frac{\alpha_t}{\alpha_0} R$$

where

$$R = \frac{\frac{3}{2}k^2\bar{k}^2 F(k, \pi/2)}{[(1 + k^2) E(k, \pi/2) - k^2 F(k, \pi/2)]}$$

This is the same ratio employed in the free-flight reduction with θ_0 replaced by α_0 . Even greater accuracy could be expected in the free-oscillation case than for free-flight reduction as there are no approximating assumptions on lift and drag terms.

D. Dynamic-Stability Testing Capabilities

The free-oscillation technique allows the acquisition of large amounts of highly accurate data in relatively short periods of time. In contrast to the free-flight technique, data acquisition and reduction are completely automatic from the wind-tunnel test to reduced data plots. This allows complete parametric studies of a

particular configuration within the capabilities of the wind tunnels. Through complementary use of the free-flight technique, a good assessment of sting effects is available for data verification. Thus, the combination of the two techniques comprise a powerful experimental tool.

Two major difficulties can arise in the employment of this technique. They are bearing friction and angle-of-attack limitations. The first problem may be minimized by the construction quality of the bearing. Damping due to bearing friction for the sting-supported air bearing described in this Report may be neglected in most cases. It represents less than 0.1% of the damping of a sharp 10-deg cone. The second problem could be alleviated by using a transverse supported bearing which would allow 360 deg of rotation. However, the problem of support interference becomes more acute in this case.

It is possible to design a spherical gas bearing which would allow 3 deg of angular freedom, up to some limited total angle of attack. Thus, a free-oscillation technique could also be extended to a nonplanar situation. Preliminary study of such a system has been initiated.

IV. SUMMARY

Two dynamic-stability testing techniques have been described in this Report. The content is complete enough to serve as a handbook for a test program, from planning and design through data reduction. Special emphasis is placed on the problem of data reduction for an axisymmetric body in planar motion. An energy integral approach, developed in Ref. 3, is applied to handle the nonlinear problems. Complete details are worked out for a specific set of nonlinear aerodynamics: a cubic pitching moment, and arbitrary lift and drag curves. This choice was made because of its wide range of applicability

to practical cases. The final results are presented in a correction factor form, which may be applied to the linear solution in order to account for the effects of the nonlinear restoring moment. By handling the solution in this fashion, it becomes particularly easy to apply it to a set of test results.

In addition, the strengths and the weaknesses of the two techniques are discussed. It is pointed out that they serve each other in a complementary fashion, and together form a very strong experimental tool.

APPENDIX A

Approximate Equations of Motion

For free-flight model design purposes only, the following approximate equations may be used to determine expected model motion. In solving the equations, the following assumptions will be made: constant dynamic pressure, small angular excursions, linear pitching moment, and single-degree-of-freedom angular oscillations about a point. The equations are:

$$m\ddot{X} - C_D q_\infty A = 0$$

$$I\ddot{\alpha} - (C_{m_q} + C_{m_{\dot{\alpha}}}) q_\infty \frac{Ad^2}{V_\infty} \dot{\alpha} - C_{m_\alpha} \alpha q_\infty Ad = 0$$

Solutions yield the following useful relationships:

1. Model Acceleration

$$\ddot{X} = \frac{q_\infty C_D A}{m}$$

2. Time to travel distance S

$$t = \left(\frac{2Sm}{q_\infty C_D A} \right)^{1/2}$$

3. Model velocity at distance S

$$V_m = \left(\frac{2Sq_\infty C_D A}{m} \right)^{1/2}$$

4. Number of oscillation cycles in distance S

$$N = \frac{1}{\pi} \left(\frac{-C_{m_\alpha}}{C_D} S \frac{d}{2} \frac{m}{I} \right)^{1/2}$$

5. Oscillation frequency

$$f = \frac{1}{2\pi} \left(\frac{-C_{m_\alpha} Ad q_\infty}{I} \right)^{1/2}$$

6. Decay in oscillation amplitude

$$\frac{\alpha_t}{\alpha_0} = \exp \left[\{C_{m_q} + C_{m_{\dot{\alpha}}}\} \frac{q_\infty Ad^2}{2IV_\infty} t \right]$$

APPENDIX B

Derivation of Least-Squares Equations for
Nonlinear Pitching Moment Fit

Given a tabulated set (n points) of data, $(C_{m_{\alpha_{eff}}})_i$ and θ_{0_i} , and the desired functional form

$$(C_{m_{\alpha_{eff}}})_i = \frac{(C_{m_\alpha} + r_m \theta_{0_i}^2) \pi^{1/4}}{[F(k_i, \pi/2)]^2} = G(\theta_{0_i}; C_{m_\alpha}, r_m) \quad (B-1)$$

where

$$k_i^2 = \frac{-\theta_{0_i}^2}{C_{m_\alpha}/r_m + \theta_{0_i}^2}$$

and F is the Legendre canonical form of an elliptic integral of the first kind, the problem is to find a C_{m_α} and r_m such that the following quantity is minimized:

$$Q = \sum_{i=1}^n \left[(C_{m_{\alpha_{eff}}})_i - \frac{(C_{m_\alpha} + r_m \theta_{0_i}^2) \pi^{1/4}}{[F(k_i, \pi/2)]^2} \right]^2$$

The method employed is the Gauss method which consists essentially of linearizing the problem with truncated Taylor series, using initial estimates of the parameters in the linear expansion to obtain new estimates, and

repeating this process until some convergence criterion is satisfied.

Therefore, suppose initial estimates $C_{m_{\alpha_0}}$ and r_{m_0} are given. Expanding Eq. (B-1) in a first order Taylor series about this point,

$$\begin{aligned} (\Delta C_{m_{\alpha_{eff}}})_i &= (C_{m_{\alpha_{eff}}})_i - \frac{(C_{m_{\alpha_0}} + r_{m_0} \theta_0^2) \pi^2 / 4}{[F(k_i, \pi/2)]^2} \\ &= \frac{\partial G(\theta_0; C_{m_{\alpha_0}}, r_{m_0})}{\partial C_{m_{\alpha_0}}} \Delta C_{m_{\alpha}} \\ &\quad + \frac{\partial G(\theta_0; C_{m_{\alpha_0}}, r_{m_0})}{\partial r_{m_0}} \Delta r_m \end{aligned}$$

The indicated partial derivatives are given by

$$\frac{\partial G}{\partial C_{m_{\alpha_0}}} = \frac{\pi^2 / 4}{[F(k, \pi/2)]^2} - \frac{\pi^2 / 2 (C_{m_{\alpha_0}} + r_{m_0} \theta_0^2)}{[F(k, \pi/2)]^3} \frac{\partial F(k, \pi/2)}{\partial C_{m_{\alpha_0}}}$$

$$\frac{\partial G}{\partial r_m} = \frac{\theta_0^2 \pi^2 / 4}{[F(k, \pi/2)]^2} - \frac{\pi^2 / 2 (C_{m_{\alpha_0}} + r_{m_0} \theta_0^2)}{[F(k, \pi/2)]^3} \frac{\partial F(k, \pi/2)}{\partial r_{m_0}}$$

where

$$\frac{\partial F(k, \pi/2)}{\partial C_{m_{\alpha_0}}} = - \frac{1/2 (r_{m_0} \theta_0^2)^{1/2}}{(-C_{m_{\alpha_0}} - r_{m_0} \theta_0^2)^{3/2}} \frac{dF(k, \pi/2)}{dk}$$

$$\begin{aligned} \frac{\partial F(k, \pi/2)}{\partial r_{m_0}} &= \frac{\theta_0^2}{2} \left[\frac{1}{(r_{m_0} \theta_0^2)^{1/2} (-C_{m_{\alpha_0}} - r_{m_0} \theta_0^2)^{1/2}} \right] \\ &\quad - \frac{(r_{m_0} \theta_0^2)^{1/2}}{(C_{m_{\alpha_0}} - r_{m_0} \theta_0^2)^{3/2}} \frac{dF(k, \pi/2)}{dk} \end{aligned}$$

$$\frac{dF(k, \pi/2)}{dk} = \frac{E(k, \pi/2) - (1 - k^2) F(k, \pi/2)}{k(1 - k^2)}$$

and E is the Legendre Canonical Form of an elliptic integral of the second kind.

This is now a linear least-squares problem with $\Delta C_{m_{\alpha_{eff}}}$ as the independent variables, and $\Delta C_{m_{\alpha}}$ and Δr_m as the parameters to be estimated. The standard linear normal equations are

$$\begin{aligned} \Delta C_{m_{\alpha}} \sum_{i=1}^n \left(\frac{\partial G_i}{\partial C_{m_{\alpha_0}}} \right)^2 + \Delta r_m \sum_{i=1}^n \left(\frac{\partial G_i}{\partial C_{m_{\alpha_0}}} \frac{\partial G_i}{\partial r_{m_0}} \right) \\ = \sum_{i=1}^n \left[(\Delta C_{m_{\alpha_{eff}}})_i \frac{\partial G_i}{\partial C_{m_{\alpha_0}}} \right] \end{aligned}$$

$$\begin{aligned} \Delta C_{m_{\alpha}} \sum_{i=1}^n \left(\frac{\partial G_i}{\partial C_{m_{\alpha_0}}} \frac{\partial G_i}{\partial r_{m_0}} \right) + \Delta r_m \sum_{i=1}^n \left(\frac{\partial G_i}{\partial r_{m_0}} \right)^2 \\ = \sum_{i=1}^n \left[(\Delta C_{m_{\alpha_{eff}}})_i \frac{\partial G_i}{\partial r_{m_0}} \right] \end{aligned}$$

Solving these 2 linear equations for the two unknowns $\Delta C_{m_{\alpha}}$ and Δr_m gives values to modify $C_{m_{\alpha_0}}$ and r_{m_0} :

$$C_{m_{\alpha_1}} = C_{m_{\alpha_0}} + \Delta C_{m_{\alpha}}$$

$$r_{m_1} = r_{m_0} + \Delta r_m$$

These improved estimates are used to repeat the process until, after q iterations, the values of $\Delta C_{m_{\alpha}}$ and Δr_m are less than some predetermined convergence criterion.

NOMENCLATURE

A	model reference area, $\pi d^2/4$	t	time
a	acceleration along model center line (see Table 1)	X	model position relative to media along tunnel centerline
C_D	drag coefficient, drag force/ $q_\infty A$; C_{D_0} = drag coefficient at zero angle of attack	V	model velocity relative to media
C_L	lift coefficient, lift force/ $q_\infty A$; C_{L_α} = lift coefficient slope per radian	V_m	model velocity relative to inertial system
C_m	pitching moment coefficient, pitching moment/ $q_\infty A d$; C_{m_α} = pitching moment coefficient slope per radian	V_∞	free-stream velocity
$\{C_{m_q} + C_{m_{\dot{\alpha}}}\}$	dynamic-stability coefficient, assumed constant over an oscillation cycle:	Z	model position in vertical direction
$\frac{\partial C_m}{\partial \frac{(\dot{\theta}d)}{V}} + \frac{\partial C_m}{\partial \frac{(\dot{\alpha}d)}{V}}$		α	model angle of attack
		α_0	initial oscillation amplitude
		$\bar{\alpha}_0$	effective oscillation amplitude
		δ^2	mean-square angle of attack
		$\delta\alpha, \delta\theta$	amplitude decay
		θ	angle between free-stream velocity vector and model centerline
d	model diameter, reference length	ρ	gas density
f	oscillation frequency, cps	Ω	oscillation frequency, radians per distance X traveled
g	acceleration due to gravity	(\cdot)	derivative with respect to time
k	modulus of elliptic integrals	$(')$	derivative with respect to distance
\bar{k}	complementary modulus	SUBSCRIPTS	
I	model moment of inertia about a transverse axis at center of gravity		
m	model mass	eff	effective constant
q_∞	free-stream dynamic pressure	l	linear
r_b	base radius of model (see Table 1)	n	nonlinear
r_m	cubic term in nonlinear pitching moment	0	condition at time or distance 0
r_n	nose radius of model (see Table 1)	t	condition at time t
		x	conditions at distance X
		∞	free-stream conditions

REFERENCES

1. Dayman, Jr., Bain, *Simplified Free Flight Testing in a Conventional Wind Tunnel*, Technical Report No. 32-346, Jet Propulsion Laboratory, Pasadena, California, October 1962.
2. Holway, H. P., Herrera, J. G., Dayman, Jr., Bain, *A Pneumatic Model Launcher for Free Flight Testing in a Conventional Wind Tunnel*, Technical Memorandum No. 33-177, Jet Propulsion Laboratory, Pasadena, California, March 1964.
3. Jaffe, Peter, *Obtaining Free Flight Dynamic Damping of an Axially Symmetric Body (at All Angles of Attack) in a Conventional Wind Tunnel*, Technical Report No. 32-544, Jet Propulsion Laboratory, Pasadena, California, January 1964.
4. Byrd, Paul F., and Friedman, Morris D., *Handbook of Elliptic Integrals for Engineers and Physicists*, Springer-Verlag, Berlin, 1954.